

Review

A review of progress and challenges in the research developments on organic solar cells

Walia Binte Tarique^{*}, Ashraf Uddin^{**}

School of Photovoltaic and Renewable Energy Engineering, University of New South Wales, Sydney, NSW, 2052, Australia

ARTICLE INFO

Keywords:

Organic solar cell
Power conversion efficiency
Non-fullerene acceptor
Stability

ABSTRACT

Solar energy, being renewable and pollution-free, has opened the path for compensating for the exploitation of non-renewable energy sources via advancements in photovoltaic technology. Solar cells have made a lot of progress over time, which has made them smaller in size and more efficient. The development of novel acceptor and donor materials, interfacial materials for better charge-carrier collection, and optimization of phase-separation morphology contribute to remarkable enhancements in the power conversion efficiency (PCE) of organic solar cells (OSCs) has reached 19%. Several challenges remain in the way of achieving PCEs of more than 20%. However, maintaining the long-term stability and higher efficiency of OSCs compared to other types of solar cells is still a major impediment to their commercialization. The fundamental design, current advances in organic materials, operation of organic photovoltaic cells, critical features of their performance, and recent work in understanding the degradation processes of OSCs are reviewed and discussed in this paper. In addition, the challenges that remain to solve in the OSCs area are also discussed.

1. Introduction

The global energy requirements are rapidly increasing in every sector of human life and industrial activities. Fossil fuel-based energies nowadays fulfill most energy requirements; however, these non-renewable energy sources are responsible for severe damage to the environment by producing a lot of greenhouse gases and pollutants, which are detrimental to lives. As a result, renewable energy development has been chosen to address energy deficiency issues by utilizing our most abundant energy source, sunlight, and solar photovoltaic (PV) technology has emerged as being one of the most promising and dependable ways to generate clean energy in the 21st century [1,2].

Organic bulk heterojunctions (BHJ) have demonstrated great application possibilities in transparent solar cells, flexible photovoltaic devices, and indoor photovoltaic devices (lightweight, flexible, high optical transparency, etc.) due to their unique material properties [3]. In recent years, organic solar cells (OSCs) have advanced significantly because of rational material design and device engineering [4–6], and the PCE of OSCs' has reached 19% [7]. Over the past 16 years, the PCE and the number of publications of OSCs have changed, as shown in Fig. 1a, meaning that research interest in OSCs is increasing day by day.

Fig. 1b illustrates a timeline of how OSCs efficiency has changed throughout time. Even though OSCs have made great advancements in recent years, reaching PCEs of 20% or more still has several numbers of significant challenges. Which limits OSCs technology to become commercially applicable like other solar cells. The poor stability of OSCs is another major barrier to the commercialization of this technology which is being studied extensively to increase the device stability.

Fig. 2 depicts the classification of OSCs into single layer, bilayer, bulk heterojunction (BHJ), ternary, and tandem structures based on the active layer structure. In 1958, Kearns and Calvin reported the very first single layer organic photovoltaic cell (Fig. 2a) [8]. Due to poor charge separation, the maximum output power was only 3×10^{-12} W. However, the PCE of the single-layer devices was less than 0.1% because it was challenging to separate excitons (pairs of electrons and holes) efficiently, and there was a lot of recombination of electrons and holes [9]. The first bilayer solar cell was reported by Tang in the year 1986 (Fig. 2b). Unfortunately, the PCE could only reach 1% due to inadequate charge transport and a deficiency of interfacial area [10]. To confront the issues of low exciton lifetime and restricted exciton diffusion length, Heeger and his colleagues developed the concept of BHJ in 1995 [11]. The BHJ structure is a combination of acceptor and donor materials

^{*} Corresponding author.^{**} Corresponding author.E-mail addresses: w.binte_tarique@unsw.edu.au (W.B. Tarique), a.uddin@unsw.edu.au (A. Uddin).

(Fig. 2c) to create an interconnected network with a wide interfacial area, which facilitates effective exciton dissociation. The diffusion distance for separating excitons improved the device's performance. The PCE of BHJ OSCs is currently reaching close to 20% [12], which was a revolution in OSCs, making it a potential PV technology.

Constructing ternary solar cells (Fig. 2d) and tandem solar cells (Fig. 2e) is a helpful way to improve the performance of the solar cells by getting the benefit of the advantages of the three parts, such as tuning the energy level, broadening the light-harvesting spectrum, and changing blend morphology [13,14]. In ternary OSCs, the combination of donors and acceptors in the active layer can be either donor: acceptor: acceptor (D:A1:A2) or donor:donor:acceptor (D1:D2:A). Photovoltaic performance can be improved in a number of ways by introducing a third donor or acceptor, such as by minimizing energy loss for improved open circuit voltage (V_{OC}) or by modifying the active layer morphology of ternary OSCs to increase fill factor (FF) [15,16]. In a tandem solar cell, an intermediate layer is placed, which provides a junction, and more charge carriers accumulate at the different electrodes. Additionally, tandem solar cells extract more sunlight because of the sub-cell, thus, resulting in more efficiency than other devices [13,17].

Bulk heterojunction (BHJ) OSCs have been the most rapidly developed and widely used type of OSC in the recent two decades. In Table 1 some recent photovoltaic performances of BHJ OSCs devices are shown. In BHJ OSCs active layer has a combination of at least two organic semiconductors, such as conjugated polymer as a donor and acceptor.

These organic semiconductor materials could be fullerene derivatives, non-fullerene derivatives, or electron-accepting polymers. This active layer is sandwiched between low-work function Al, Ag, or Ca metal cathodes and transparent ITO anode electrodes. In addition, a few transition metal oxides semiconductors, such as ZnO, TiO₂ have been used as electron transport layers (ETL) and PEDOT:PSS, MoO₃ as hole transport layers (HTL) to extract the charge carriers properly [18–23].

In a basic solar cell device, incident photons from the sunlight are converted into electrical current. The device's operation consists of four critical steps: in four stages: (i) absorption of the incident photon and exciton generation (ii) exciton diffusion (iii) dissociation of excitons due to high electron affinity of acceptors and (iv) charge collection at electrodes Fig. 3.

First, the incident photon is absorbed by the active layer after passing through the transparent electrode. Like the conduction and valence bands of inorganic semiconductors, polymers with the suitable highest occupied molecular orbital (HOMO) and lowest unoccupied molecular orbital (LUMO) energy levels are utilized as a donor in OSCs. Excitons are formed when an electron is excited from the HOMO to the LUMO, producing a bound electron-hole pair with a high coulombic interaction energy (exciton binding energy). Since organic materials have a low dielectric constant ($\epsilon_r \approx 2–3$), it is more difficult to overcome the strong coulombic attraction between an electron and a hole [24,25]. Due to the high binding energy of the electron-hole pair (0.1–1.0 eV), an exciton must have a built-in field to split into free electrons. The holes have

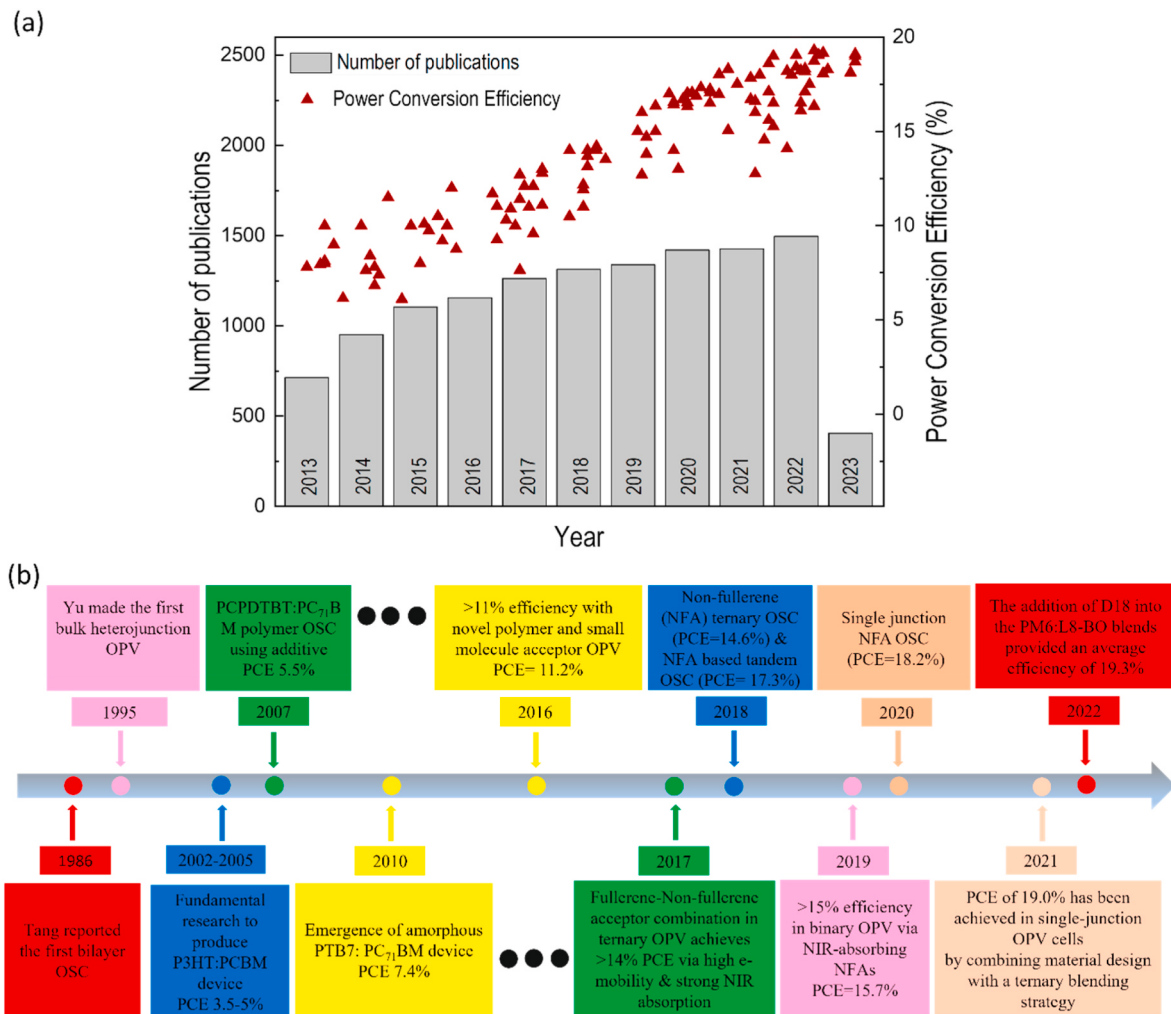


Fig. 1. (a) Shows the development of power conversion efficiencies and the number of publications on organic solar cells from 2005 to 2021. (Data obtained from Scopus). (b) A timeline of the progress of OSCs efficiency. The boxes represent the materials and device configurations used to develop the PCE of OSCs.

distinct ionization potentials and electron affinities [26,27].

Exciton binding energy (E_b), which corresponds to the energy conversion from exciton to free hole and electron charge carriers, is one of the major elements determining the operating mechanisms and performance of organic optoelectronic devices. E_b is the energy difference between the fundamental transport gap (E_g^t) and the optical gap (E_g^o): $E_b = E_g^t - E_g^o$ [28], where E_g^t is defined as the difference between the electron affinity (E_A) and ionization potential (IP), and E_g^o is the excitation energy from the ground state (S_0) to the first singlet excited state (S_1).

Due to the energy gap between the LUMO levels of the donor and acceptor materials, excitons dissociate into free electrons and holes. The diffusion lengths are restricted to the nanoscale range because most conjugated polymers generate excitons with short lifetimes (less than 20 nm). Therefore, for efficient charge creation, excitons need to be created inside of its diffusion length (LD). The charge transfer efficiency (η_{CT}) is defined as the number of excitons that have transferred charges at the D/A interface to the total number of excitons. As a result of exciton dissociation, electrons and holes are generated and transferred to the electrodes via the donor and acceptor [30–33]. Free carrier charge transport occurs in a timescale of nanoseconds. Charge carriers recombining before reaching their respective electrodes is one of the major factors that make it difficult for them to move toward the hole and electron contacts. When the active layer gets too thick, free carriers are more likely to recombine, leading to reduce the performance of OSCs. It is also crucial to decrease the recombination loss for achieving high-performance OSCs [34–36].

Generally, the open-circuit voltage (V_{OC}), fill factor (FF) and short-circuit current density (J_{SC}) of solar cells are defined by the current density and voltage (J-V) properties of the solar cells [37–39]. All of these parameters have intimate connections to the photoactive materials (acceptor and donor materials). The number of free carriers accumulated at the electrodes at zero applied potential (when $V_{OC} = 0$) is known as the short circuit current density (J_{SC}). The energy difference between the HOMO and LUMO of the acceptor and donor materials determines the highest voltage that a solar cell may extract for an external circuit is referred to as the open circuit voltage (V_{OC}) [40–42]. Also, Fill-Factor (FF) is the degree of the shape of current and voltage characteristics of OSCs. It represents how close the shape of the output characteristic is to the ideal device characteristic [42].

The power conversion efficiency (PCE) is the ratio of output power that a solar cell can produce to the input power (equation (1)), which is described by the J_{SC} , V_{OC} , and FF as follows:

$$PCE = \frac{J_{SC} \times V_{OC} \times FF}{P_{in}} \quad (1)$$

Table 1
Photovoltaic performances of BHJ type binary OSCs devices.

Donors	Acceptors	V_{OC} [V]	J_{SC} [mA cm ⁻²]	FF [%]	PCE [%]	Ref.
PFBDB-T	C8-ITIC	0.94	19.6	72	13.2	[45]
PBDB-TF	BTP-eC9	0.841	26.2	78.3	17.3	[46]
P3HT	IC ₇₀ BA	0.87	11.53	75.0	7.40	[47]
PM6	Y6	0.83	25.63	68.40	14.55	[48]
PM6	Y6	0.85	24.45	72.69	15.10	[49]
PBDF-NS	Y6	0.728	26.88	72.9	14.26	[50]
PBB-T	ITIC-F	0.91	20.9	70	13.3	[51]
PBDB-T-SF	IT-4F	0.88	20.50	71.9	13	[52]
PBDB-T	IT-M	0.94	17.44	0.735	12.05	[53]
PTB7-Th	IEICO-4F	0.71	27.3	66	12.8	[54]
PM6	BTP-eC9-16	0.844	27.78	77.68	18.20	[55]
PBQx-TF	eC9-2Cl	0.879	27.2	80.4	19.20	[56]
PM6	Y6	0.82	25.2	76.1	15.7	[57]
PM6	IPTBO-4Cl	0.893	23.15	72.57	15.00	[58]
PBDB-T	ITIC	0.932	17.97	66.2	11.21	[59]
T26T	eC9-4F	0.863	25.14	70.86	15.38	[60]
BTR-Cl	Y6	0.86	24.17	65.5	13.61	[61]
PTQ10	MO-IDIC-2F	0.906	19.87	74.8	13.46	[62]
PBDB-T	IDT-EDOT	0.86	21.34	62.0	11.32	[63]
D18	Y6	0.859	27.70	76.6	18.22	[64]
D18-Cl	Y6	0.87	27.52	75.59	18.15	[65]

In OSCs, high J_{SC} is achievable when the donor materials have a small optical bandgap (E_g), and the V_{OC} is determined by the energy gap between the HOMO of the donor materials and the LUMO of the acceptor materials. Also, electrically well-aligned material structures facilitate the movement of charge carriers, which reduces charge carriers' recombination in active layers and increase the FF of OSCs. To get high PCEs in OSCs, many studies have been done over the past 20 years on how to make small E_g donor materials with highly crystalline structures [43,44].

The development of OSCs has heavily depended on the usage of fullerenes and their derivatives as electron acceptors during the past 20 years. Their delocalized lowest unoccupied molecular orbital (LUMO) electrical properties provide them with strong electron mobility, and their three-dimensional molecular structures qualify them for BHJ structures. High-efficiency OSC devices can develop excellent percolation when coupled with donor molecules like suitable conjugated polymers [66–68]. But organic solar cells with fullerene acceptors don't work as well as they could because fullerene acceptors have some problems. Because of their highly symmetrical chemical structure and difficulty in being synthesized, fullerene acceptors are not very good at

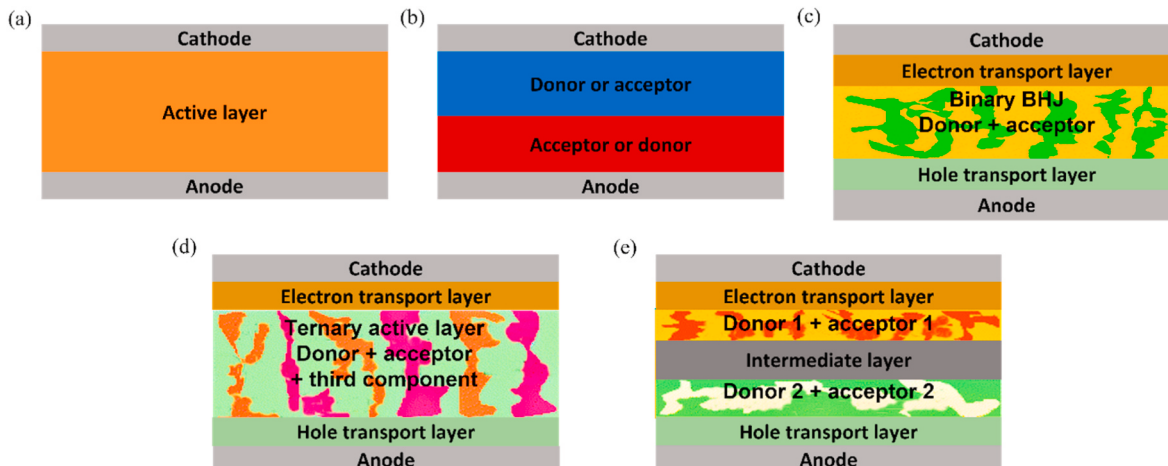


Fig. 2. Schematic diagrams of different OSC device structures.

Table 2

Some of the donor & acceptor combinations (A1:A2:D or D1:D2; A) of ternary blend OSC devices' photovoltaic performances.

Ternary blend active layer	Configuration/ratio	V_{OC} [V]	J_{SC} [mA cm^{-2}]	FF [%]	PCE [%]	Ref.
PM6:SM1:Y6	DDA/0.85:0.15:1.2	0.831	25.70	77.50	16.55	[80]
PM6:BPR-SCL:Y6	DDA/0.75:0.25:1	0.870	25.77	75.00	16.74	[115]
PTB7-Th:TR:FOIC	DDA/1:0.25:1.5	0.734	25.1	70.9	13.1	[82]
PM6:J71:Br-ITIC	DDA/0.8:0.2:1	0.930	19.39	78.4	14.13	[116]
PM6:DRTB-T-C4:Y6	DDA/1:0.15:1.2	0.850	24.8	81.3	17.13	[83]
PM6:S3:Y6	DDA/0.8:0.2:1.2	0.856	25.86	79.17	17.53	[84]
PBDB-TF:PB2F-BTP-eC9	DDA/0.8:0.2:1.2	0.863	26.8	80.4	18.6	[85]
PBDB-T:PTB7-Th:FOIC	DDA/0.5:0.5:1	0.73	24.61	65.51	12.02	[86]
PM6:Y6:BTP-M	DAA/1:1:0.2	0.875	26.56	73.46	17.03	[87]
PM6:Y6:3TP3T-4F	DAA/1:1.02:0.1	0.85	26.10	75.4	16.7	[117]
PBDB-TF:HDO-4Cl:eC9	DAA/1:0.2:1	0.866	27.05	80.5	18.86	[118]
PM6:BTP-S2:BO-4Cl	DAA/1:0.3:0.9	0.861	27.14	78.0	18.2	[119]
PM6:IT-4F:N7IT	DAA/1:0.7:0.3	0.890	22.54	74.8	15.02	[120]
PM6:Y6:IDIC	DAA/1:1:0.2	0.868	25.39	74.92	16.50	[121]
PM6:ICBA:IT-4F	DAA/1:0.1:0.9	0.88	21.25	76.55	14.25	[122]
PM6:L8-B0-eC9-2Cl	DAA/1:0.8:0.2	0.89	26.63	78.7	18.66	[123]
B1:BO-4Cl:L8-BO	DAA/1:0.2:0.8	0.841	26.15	77.74	17.10	[124]
PM6:D18:LB-BO	DDA/0.8:0.2:1.2	0.89	26.7	82	19.3	[125]
PM6:D18-Cl:LB-BO	DDA/0.7:0.3:1.2	0.91	26.66	79.24	19.22	[126]

absorbing light, especially in the ultraviolet, visible, and near-infrared ranges. This makes it very hard for fullerene acceptor-OSCs to generate photocurrent. Also, fullerenes have fixed energy levels that are hard to change, making it harder for them to work well with polymers with different energy levels.

Blending donor materials with nanoscale-interpenetrating morphology is also a challenging but significant element to consider. Moderate aggregations are the preferred form. Small aggregate domains

minimize optical absorption and charge transfer, whereas large aggregations diminish excitons separation efficiency and induce geminate recombination losses. Changes in molecular structures, rather than conformations, seemed to be an effective method for modifying crystallinity. Carrier mobility may be improved by increasing the crystallinity and therefore enhancing noncovalent forces such as van Der Waals and hydrogen-bonding interactions. A better way to make molecules more soluble is to introduce side chains, minimize inter-and intramolecular interactions, and distort the conformation of molecules [69, 70]. Intramolecular noncovalent bonds (weak intramolecular interactions like S...O, S...F, and Se...O) offer a promising technique to tune the electronic properties and solid-state molecular packing of π -conjugated molecules by providing more precise control over their conformation. Because of the locked conformation, the molecular rigidity is increased and the backbone developed more planar, which enables more effective π -conjugation, orderly intermolecular stacking, and less internal reorganization energy [71–74].

Alternately, building ternary mix OSCs by introducing a third component, either polymer acceptor (A) or donor (D), is a viable technique for achieving prolonged light absorption in a single-junction device by combining the benefits of binary and tandem OSCs. Due to the restricted choice of acceptors, early efforts at developing ternary mix OSCs concentrated mostly on fullerene acceptor (FA)-based 2D/1A-type devices. The number of novel non-fullerene acceptors (NFAs) inventions has increased dramatically in recent years, which has led to the progression of the non-fullerene acceptor (NFA)-based ternary mix OSCs (NFTSCs) [75–80]. Also, the formation of the highly efficient ternary system depends on its third component, which must have been good chemical and electronic compatibility with the other two host materials. For example, a D18-Cl donor was combined with two structurally related Y6 derivatives (Y6 and Y6-1O) as dual acceptors. The addition of this third element improved photon harvesting capability, helped to reduce energy loss, and changed the shape of the ternary BHJ. For these reasons, D18-Cl:Y6:Y6-1O based ternary OSC produced high efficiency of 17.91%. Besides, the open-circuit voltage (V_{OC}), short-circuit current (J_{SC}) and fill factor (FF) all increased at the same time. By using the ternary strategy, the performance of OSCs has been boosted. However, in most cases, efficient ternary OSCs are used with one donor and two congruent acceptors (D:A1:A2). In contrast, ternary systems with two congruent donors (D1:D2:A) are rarely studied due to a lack of suitable materials [81–88].

Interface engineering of OPV cells plays a crucial role in enhancing the performance of the device [23, 89, 90]. First, choosing a suitable interface material may decrease the device's resistance, and the device's light harvesting and carrier transport capabilities can be enhanced, hence enhancing PCEs. Second, suitable interface materials may significantly improve the device's stability by isolating the active layer from water, oxygen, and other unfavorable components of the external environment. Finally, proper interface materials must match the

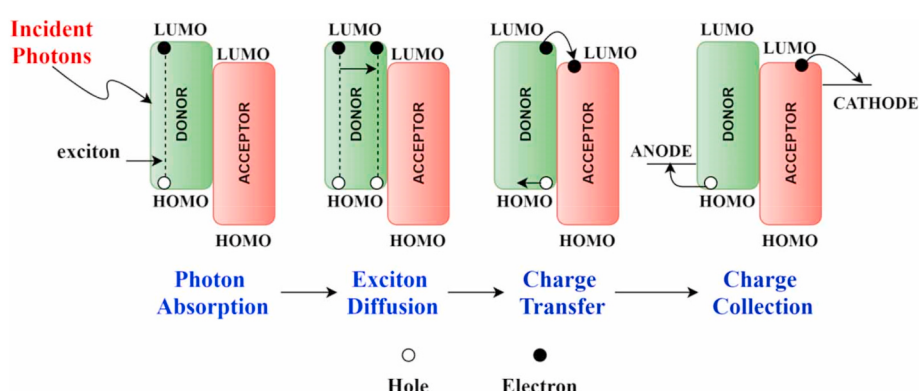


Fig. 3. Working mechanism of bulk-heterojunction OSCs. Reproduced with permission [29]. Copyright 2021, IOP Publishing Ltd.

commercialization criteria of OPVs to simplify processing technology and reduce production costs. A critical review of OSC's updated progress achieved in the device performance as well as its stability is needed for researchers to better understand and solve the stability bottleneck toward commercialization.

In this review, we have focused on the aspects that affect the efficiency and stability of OSCs. Firstly, the solar cell attributes, such as short circuit current (J_{SC}), open-circuit voltage (V_{OC}), and fill factor (FF), is discussed as the working principle of OSC. Secondly, the role of narrow bandgap donors, acceptors, and non-fullerene acceptors (NFAs) materials is discussed, which are frequently used as an active layer in the OSCs. Thirdly, the degradation factors of OSCs responsible for device instability are discussed. Finally, we propose some prospects, challenges, and outlooks for the future commercialization of OSCs.

2. Recent approaches in enhancing device efficiency of OSCs

Because of these developments, new acceptor and donor materials are being used in BHJ blends, tandem devices, and other more complex OSC structures. Additionally, more favorable interfacial layers and enhanced morphological control are crucial factors. This section summarises the emergence of various high-efficiency OSC approaches.

2.1. Developments in acceptors

In the beginning, OSCs depended heavily on $PC_{61}BM$ and $PC_{71}BM$ fullerene derivatives electron acceptor materials because of their excellent electron mobility, strong electron affinity, and isotropic charge transfer. Despite the rapid advancement of OSCs with fullerene acceptors, their efficiency is limited by their low intrinsic absorption, high voltage losses (V_{loss}), the untenability of energy levels, and morphological instabilities [91]. To address these disadvantages, NFAs (Fig. 4) have rapidly gained popularity because of their high absorption in the

visible-near-infrared range and their readily tunable energy levels [92, 93].

Zhan's group revealed the first effective NFA, named ITIC, using an acceptor-donor-acceptor (A-D-A) structure (Fig. 5a) in 2015 based on a bulky seven-ring fused core (indacenodithieno [3,2-b]thiophene, IT), end-capped with 2-(3-oxo-2,3-dihydroinden-1-ylidene)malononitrile (INCN) groups, and with four 4-hexylphenyl groups substituted on it. The electron-withdrawing cyano and carbonyl groups in each INCN may push the LUMO level downward. Intermolecular charge transfer may be induced via ITIC's push-pull structure, which extends absorption. In BHJ OSCs, the four rigid 4-hexylphenyl substituents outside the IT major plane may limit aggregation, molecular planarity, and significant phase separation in active layers. ITIC exhibits properties such as low LUMO, high HOMO, wide absorption, efficient electron transport, wide absorption range, and good miscibility with polymer donors [21]. The first NFA-based BHJ organic solar cell, reported by Zhao et al., in 2017, exceeded the state-of-the-art in fullerenes. The PBDB-T-SF:IT-4F photoactive layer-based OSC device achieved high efficiency of 13.1%. With an extended optical absorption and increased active layer absorption coefficient, the PBDB-T-SF:IT-4F device exhibited a notable increase in J_{SC} from 17.03 to 20.50 mA/cm² compared to the PBDB-T:ITIC control device (Fig. 5b) [52].

A variety of techniques have been used by molecular engineers to produce high-performance OSCs. End groups (constituent units at the edge of an oligomer or macromolecule) modification is one of the most notable strategies for simple tuning of molecular energy-level alignment. For example, Cui et al. created BTP-4Cl-9 by attaching a 2-butylloctyl (BO) branch to the pyrrole ring of BTP-4Cl. As the alkyl chain length grows, this compound's absorbance shifts to the red owing to increased aggregation. The PCE of the PBDB-TF:BTP-4Cl-9-based device was an amazing 17.3% [46]. Chlorination is more successful than fluorination in prolonging the optical absorption, as demonstrated by the substitution of fluorine atoms from BTP-4F(Y6) with chlorine atoms

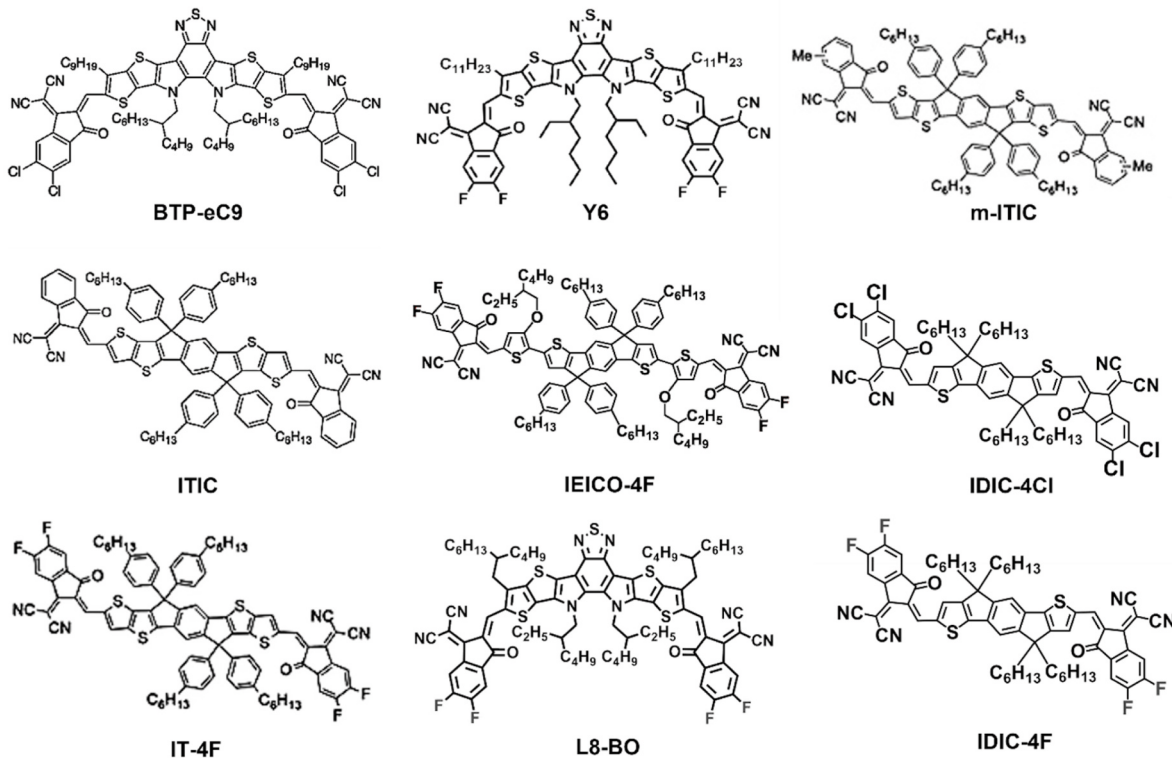


Fig. 4. Molecular structures of some important non-fullerene acceptor (NFA) materials.

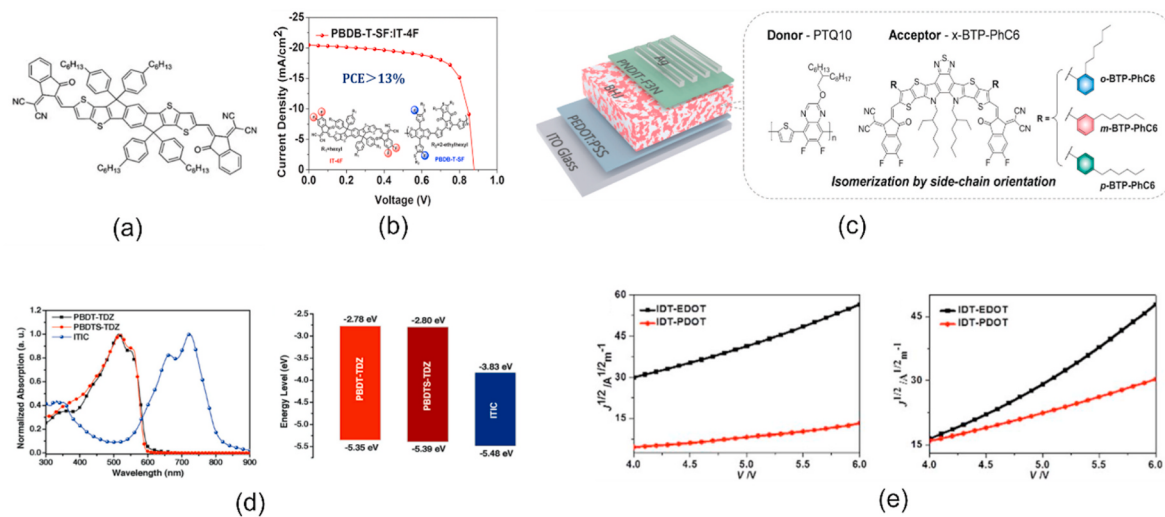


Fig. 5. (a) Molecular structure of non-fullerene electron acceptor (ITIC). Reproduced with permission [21]. Copyright 2015, John Wiley and Sons. (b) J - V curve for 60 PBDB-T-SF:IT-4F-based cells. Reproduced with permission [52]. Copyright 2017, American Chemical Society. (c) Chemical structures of the donor polymer PTQ10 and the acceptor materials, *o*-BTP-PhC6, *m*-BTP-PhC6, and *p*-BTP-PhC6. Reproduced with permission [95]. Copyright 2021, The Royal Society of Chemistry. (d) Normalized absorption of the copolymer and ITIC films and energy level diagram of the copolymers and ITIC. Reproduced with permission [96]. Copyright 2017, John Wiley and Sons. (e) Electron and hole mobility of blend films based on PBDB-T:IDT-PDOT and PBDB-T: IDT-EDOT. Reproduced with permission [62]. Copyright 2018, The Royal Society of Chemistry.

at the terminal electron-withdrawing units. The OPV cells using BTP-4Cl exhibited greater open-circuit voltages (V_{OC}). ITPBO-4Cl, an asymmetric ADA acceptor containing nitrogen, was described by Yang et al. Intramolecular charge transfer is improved when chlorine substituents are added to the terminal units. The large alkyl chain attached to the nitrogen greatly expands the backbone's stacking area and prevents the molecule's nitrogen atoms from clustering together. For IPTBO-4Cl solar cells, this configuration resulted in a PCE of 15% [58]. Cui et al. reported a chlorinated BTP-4Cl non-fullerene acceptor with enhanced optical absorption and a higher voltage in devices than its fluorinated counterpart. PCE of 16.5% is reached when OSC is used in conjunction with a BTP-4Cl/PBDB-TF active layer [94]. The work of Chai et al. mainly focused on the engineering of side-chain substitution locations for the core phenyl rings (*o*-, *m*-, and *p*-positions). The intermolecular packing in *m*-BTP-PhC6 was the most organized of the three acceptors. The three isomers are structurally distinct from one another because of where the hexyl chains are substituted (i.e., *ortho*-, *meta*-, and *para*-substitutions on the phenyl rings connected to the *b*-positions of the thienothiophene units) (Fig. 5c). The J_{SC} and FF of the devices benefit from PTQ10: *m*-BTP-PhC6 due to its proper phase separation and enhanced molecular packing, which reduces charge recombination and increases charge transport. In comparison to other PTQ10-based devices, those based on *m*-BTPPhC6 had the highest PCE at 17.7% [95]. According to the work of Li et al., SMA *m*-ITIC has *para*-hexylphenyl units replacing *meta*-hexylphenyl groups in the side chains. Higher absorption coefficient, crystalline coherence, and μ_e values in *m*-ITIC paired with donor J71 resulted in a high PCE of 11.77%.

Another well-known acceptor, IT-4F, was synthesized by adding a fluorine atom (end group modification of ITIC), which dramatically increased intramolecular contact and promoted charge transfer. The PCE of 14.7% was reached using the PTO2:IT-4F devices [97]. Feng et al. constructed an asymmetric seven-heterocyclic fused ring acceptor IDTT-OB. IDTT-OB, with its seven fused heterocyclic rings, showed higher HOMO levels, smaller band gaps, and better absorption compared to IDT-OB. The device is a combination of IDTT-OB and PBDB-T. Nanoscale phase separation in the composite membrane improved exciton transport and charge transfer. The PCE for the device achieved 11.19% [98]. Xu et al. constructed a wide-bandgap (over 2.07 eV) donor poly(2-(5-(4,8-bis(5-((2-butyloctyl)thio)thiophen-2-yl)benzo[1,2-b:4,5-b']

dithiophen-2-yl)-4-octylthiophen-2-yl)-5-(4-octylthiophen-2-yl)-1,3,4-thiadiazole) (PBDS-TDZ) with a HOMO energy level of 5.39 eV that fits well with the donor's HOMO energy level results in complementary light absorption in the 300–800 nm region. This results in significant complementary light absorption. As a result, the PCE for the PBDS-TDZ:ITIC-based OSCs is 12.35% (Fig. 5d) [96]. Yuan et al. developed Y1, a seven-membered fused-ring NFA with stronger and wider absorption from 600 to 900 nm, improved charge-transfer efficiency and lower energy levels. The PCE for the PBDB-T:Y1-based device was 13.42% [99]. Li et al. developed simple-structured fused-ring ADA acceptors MO-IDIC-2F and MO-IDIC that can be synthesized using a simpler approach with high overall yields from minimal starting materials. The highest PCE of 13.46% was attained by solar cells made with the donor material PTQ10 and the MO-IDIC-2F solar cell. This study demonstrates the enormous potential for effective organic solar cells in the form of low-cost donor and acceptor materials [61]. Jiang et al. created and synthesized two SMAs, IDT-EDOT and IDT-PDOT, both of which contain bridging units of 3,4 ethylenedioxythiophene (EDOT) and 3,4-propylidene dioxythiophene (PDOT). IDT-EDOT has higher charge mobility and a stronger capacity for light trapping than IDT-PDOT due to its conformation and dense stacking (Fig. 5e). The PCE of the IDT-PDOT-based OSC device is just 2.09%, but the PCE of the IDT-EDOT-based device is an amazing 11.32% [62].

2.2. Developments in donors

The BHJ structure is blended with electron-accepting materials (A) and electron-donating materials (D), resulting in a bi-continuous interpenetrating network nanostructure that improves exciton dissociation and charge carrier transmission. Donor materials are critical in OSCs since they are responsible for matching photons to electron acceptors and converting them to free charges. Polymers and small molecule materials are employed as donors (Fig. 6) [100,101]. Before the great success of NFAs, conjugated polymers were usually designed to match fullerene acceptors for OSCs to improve the light-harvesting ability of the active layer. On the basis of optical bandgaps E_g , donor materials can be divided into three major types: wide bandgap (WBG, $E_g > 1.8$ eV), medium bandgap (MBG, $1.6 \text{ eV} < E_g \text{ opt} \leq 1.8 \text{ eV}$), and low bandgap (LBG, $E_g \leq 1.6 \text{ eV}$) [102]. In the early days of polymer solar cell (PSC) study, WBG polymers were frequently constructed from homo

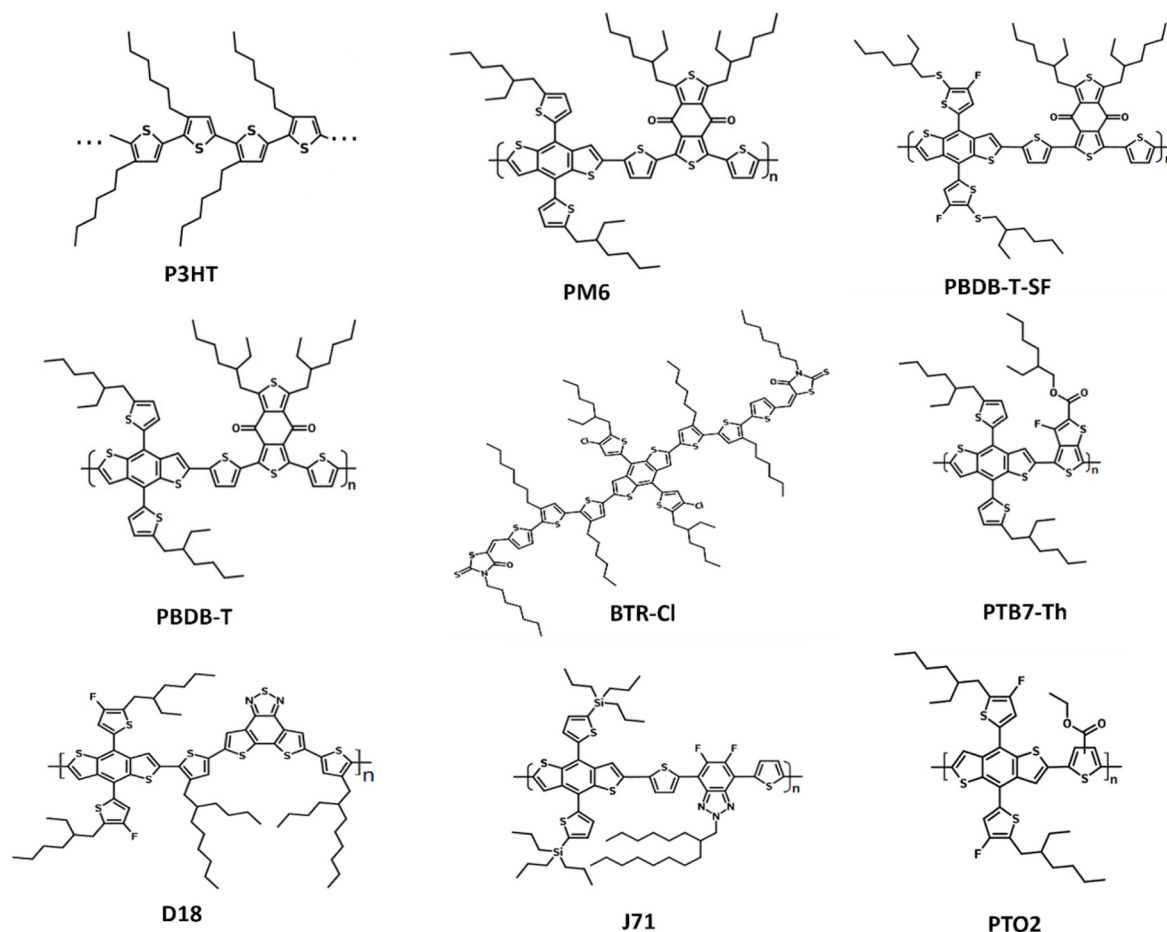


Fig. 6. Molecular structures of some important donor materials.

buildingblocks like poly(3-hexylthiophene)(P3HT) and poly[2-methoxy-5-(3,7-dimethyloctyloxy)-1,4-phenylene-vinylene] (MDMO-PPV), which were extensively explored as donors in fullerene-based PSCs [103,104]. One of the promising materials is a combination of poly(3-hexylthiophene) (P3HT) and [6,6]-phenyl C₆₁-butyric acid methylester (PCBM). So far, it is the most efficient donor-acceptor copolymer based on fullerene derivates. The active layer of OSC was initially composed of a mixture of poly(3-hexylthiophene) and 1-(3-methoxycarbonyl)-propyl-1-phenyl-[6,6]C₆₁(P3HT:PCBM) [105]. Then, the P3HT:PCBM system progressively became the most widely used material system. Numerous studies have been conducted to optimise the morphology, crystallinity, and phase separation of the active layer using solvent additives, thermal annealing, and other techniques Erb et al. analyzed the interaction between P3HT:PCBM optical characteristics and crystallinity. After annealing, the isolated PCBM molecules were diffused into bigger aggregates, whereas P3HT aggregates were converted into P3HT crystallites in these PCBM-free areas. The annealed P3HT:PCBM OSC's PCE improvement was attributed to the PCBM cluster's enhanced electron transport and higher P3HT absorption [106]. The wide bandgap donors resulted a comparatively low J_{sc} in corresponding devices, hence MBG- and LBG-donor materials were designed to enhance the PCE of OSCs. A low-bandgap polymer donor, PBDTTT-CF, with an absorption edge of 770 nm was developed and synthesized in 2009 by Chen et al. The J_{sc} of devices based on PBDTTT-CF:PC₇₁BM was 15.2 mA/cm², indicating significant photoconversion efficiency within the wavelength range of 400–700 nm. Power conversion efficiency of 7.73% was achieved as well as increased V_{oc} caused by modifying the energy level of PBDTTT-CF [107]. In 2010, Liang's group expanded the PTB family with the introduction of PTB7,

and OSCs based on PTB7:PC₇₁BM achieved a PCE of up to 7.40% [66]. Chen's group increased the PTB7 main chain coplanarity by adding a 2-ethylhexyl-thienyl group to the BDT unit in order to increase the absorption of PTB7. In comparison to PTB7, the novel copolymer PTB7-Th exhibited an optical bandgap of 1.58 eV, a decrease of 0.05 eV. An impressive PCE of 10.10% was achieved with an increase in J_{sc} from the OSC based on PTB7-Th:PC₇₁BM blends [68,108]. The ability of NFAs to absorb light is typically greater than that of fullerene derivatives. As a result, a variety of donor materials ranging from WBG to LBG could be employed in place of fullerene acceptors to produce highly efficient OSCs utilizing NFAs. The benzodithiophene-4,8-dione (BDD) unit and the benzodithiophene (BDT) unit combine to form the polymer donor PBDB-T, which has a distinctive aggregation behaviour and an extensive absorption in the short wavelength range. PSC was fabricated by combining polymer donor PBDB-T and LBG non-fullerene acceptor ITIC. The PBDB-T:ITIC blend showed a considerably broader absorption spectrum and smaller ΔE_{HOMO} and ΔE_{LUMO} than the PBDB-T:PC₇₁BM blend, which is favorable to increase solar photon harvesting ability and reduce V_{OC} loss, and consequently, it produced a remarkable PCE of 11.21% with higher J_{sc} and V_{oc} [109]. Using the small molecule acceptor IT-4F and the fluorination-synthesized polymer donor PBDB-T-SF, Zhao et al. were able to attain a PCE of 13%. Molecular energy levels in PBDB-T-SF: IT-4F materials are lower than in their nonfluorinated equivalents. The J_{SC} for the associated OSC device is much improved as a result of the expanded optical absorption range and higher absorption coefficient of the active layer [52]. Additionally, Li et al. observed that the polymeric blend PBDB-T:IT-M had a relatively high PCE of 12% [53]. Wen et al. synthesized a highly efficient OSC by combining donor polymer PBB-T with ITIC-F. PBB-T is well-known for

its strong absorption capabilities in the most significant solar radiation band, as shown by the PBB-T:ITIC-F blend's external quantum efficiency of more than 75% [51]. Modifying the side chain is a promising approach for controlling molecular packing, solubility, and film morphology. Tan et al. synthesized a sequence of terpolymers (PM10Si, PM20Si, and PM30Si) based on PM6 with varying amounts of siloxane-substituted DTBT. In comparison to PM6, these terpolymers, when blended with Y6, can provide a strong driving force for phase separation of the active layer, thus resulting in higher mobilities. An improved PCE of 15.17% and J_{SC} value of 26.972 mA/cm² were achieved using the PM20Si:Y6-based device [110]. With the acceptor Y6, the BDF-based polymer PBDF-NS displays similar absorption spectra, matching energy levels, and superb fibril network architecture, yielding a PCE of 14.26% [52].

The OSC developed by Song et al. comprised a polymer donor (PTB7-Th) and a norfullerene acceptor (IEICO-4F) with a narrowband gap as the active layer, and 1-chloronaphthalene (CN) was added as a solvent. Because of the strong (010) reflection of $\pi-\pi$ stacking in the OOP direction (Fig. 7e), the 2D GIWAXS patterns (Fig. 7a–d) and pole figures (Fig. 7f) exhibit a preferable face-on orientation for the polymer:NFA blends for all samples. Additionally, the face-on to edge-on ratios (Fig. 7g) can be extracted from pole figures of the (100) peak. To get a high scattering contrast for these NFA blends, the R-SoXS profiles (Fig. 6h) are recorded at the resonant energy (~283 eV) to get high scattering contrast for these NFA blends. Optical and electrical measurements demonstrate enhanced charge transfer and decreased recombination in optimum devices with a 4% CN addition, resulting in a 12.8% efficiency [54].

Wang et al. reported a PCE of 18.20% using a PM6 polymer donor and a BTP-4F-C5-16 non-fullerene acceptor [111]. Upama et al. achieved high-efficiency PBDB-T:ITIC non-fullerene BHJ OSCs employing a layer of ZnO nanoparticles as the ETL, achieving over 11.21% efficiency [59]. Like polymer donor-based devices, small molecule donors (SMDs) combined with non-fullerene acceptors (NFA) in non-fullerene small-molecule organic solar cells. Duan et al. discovered the Tz6T oligothiophene donor with a thiazole core. Tz6T-based binary ASM-OSCs reach a breakthrough efficiency of 15.4% by integrating the non-fullerene acceptor ec9-4F [60]. Chen et al. synthesized the liquid crystalline compound BTR-Cl by chlorinating the BTR molecule. Due to the difference in liquid crystalline characteristics between BTR-Cl donor

and Y6 acceptor materials, a PCE of 13.6% was obtained [63]. Qiu et al. studied the influence of various thiophene conjugated side chains on donor molecules' molecular aggregation, photophysical, and photovoltaic characteristics, including SM1-S with alkylthio and SM1-F with fluorine. Consequently, the PCE of SM1-F donor-derived SM-OSC is the greatest at 14.07% [112]. Zhou et al. found three small-molecule donors ZR1, ZR1-Cl, and ZR1-S-Cl based on dithieno[2,3-d:2',3'-d']benzo[1,2-b:4,5-b']dithiophene (DTBBD) unit. Among the three donors, ZR1-S-Cl achieved PCE of 12.05% with IDIC-4Cl acceptor [113]. Duan et al. fabricated ASM OSCs with 2Cl7T donor and Y6 acceptor, which delivered PCE of 11.45% [114].

2.3. Progress in ternary blend organic solar cells

Beyond one pair of acceptor-donor binary blends, ternary blend OSCs have emerged as a viable technique for simultaneously improving device efficiency and stability. Light absorption bandwidth may be expanded by combining numerous donor or acceptor materials, especially in OSCs, since ordinary organic semiconductors have an innately restricted absorption window. Ternary OSCs offer many benefits over binary mixes, including forster energy transfer, cascading energetics, and the capacity to confine electrons or holes in a high-purity phase, reducing recombination [75,76]. During active layer processing, ternary OSCs often include a third component, either an acceptor or a donor, in the binary (A:D) host system, establishing a ternary D:D:A or a D:A:A system (see Table 2). Fig. 8 shows possible combinations of the three components and the operating mechanism of a ternary system (a-b). Ternary solar cells, which use absorption spectrum complementing materials as the second acceptor or donor, are an effective and practical way to improve photon harvesting that led to a numerous significant contributions have been made to developing ternary OSCs [77–79].

2.3.1. Donor as a third component

Since conjugated polymers have relatively narrow absorption spectra, adding a polymer or small molecule donor may increase the active layer's light absorption and enhance charge dissociation and transport. Yan et al. created a ternary configuration by inserting a small molecular donor SM1 into the PM6:Y6 configuration, achieving higher efficiency of 16.55% compared to its binary counterpart (15.75%). The connection between V_{OC} and different SM1 concentrations indicated

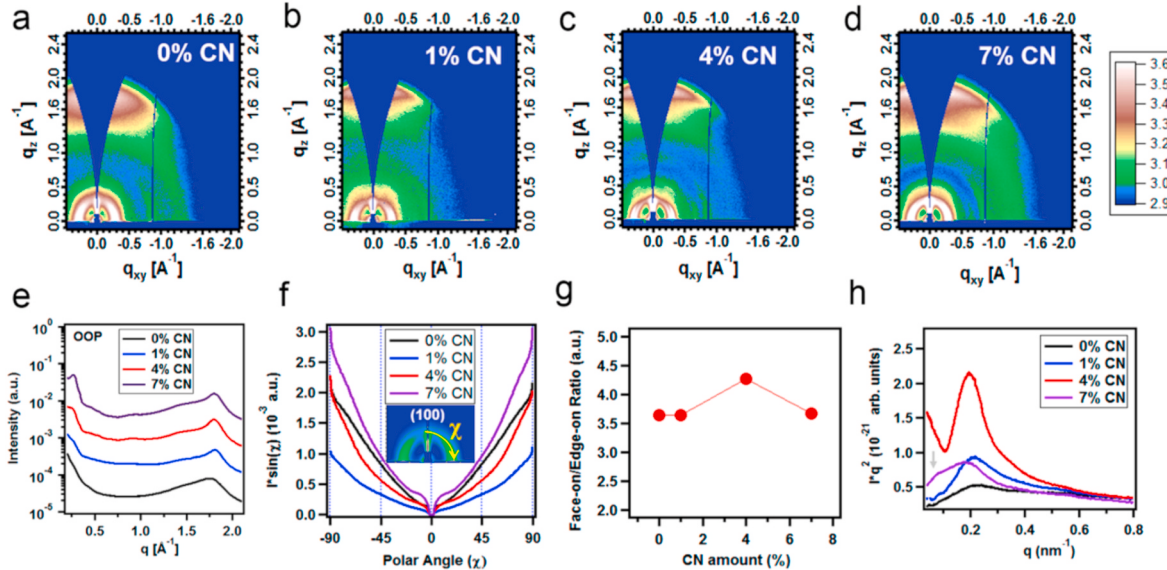


Fig. 7. Image of GIWAXS 2D patterns for the PTB7-Th:IEICO-4F blend active layer with (a) 0, (b) 1, (c) 4, and (d) 7% CN. (e) GIWAXS out-of-plane (OOP) profiles, (f) corrected pole figure of (100) peaks, (g) face-on to edge-on ratio, and (h) Lorentz corrected R-SoXS profiles of PTB7-Th:IEICO-4F blend films with different amount of CN. Reproduced with permission [54]. Copyright 2018, American Chemical Society.

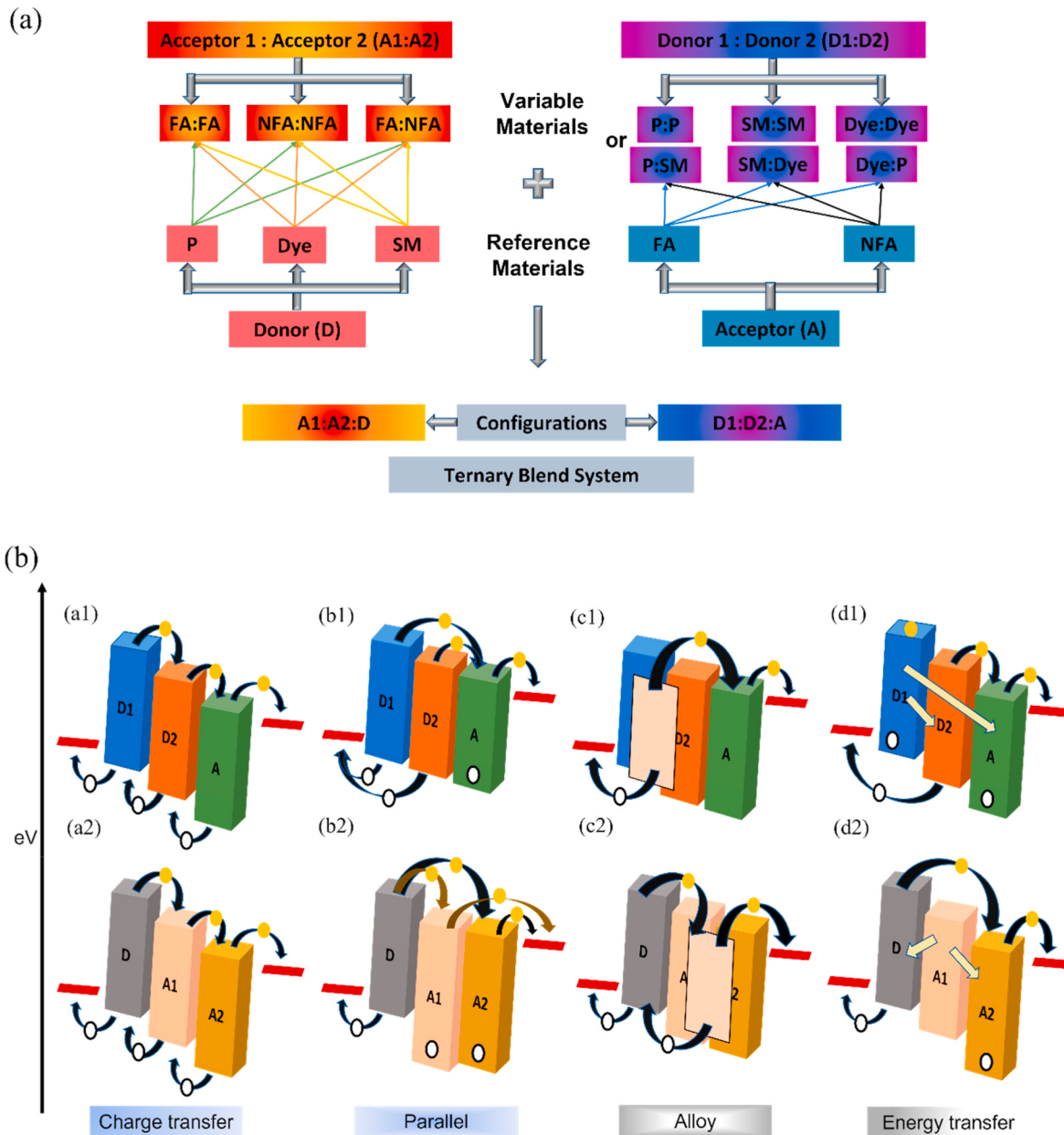


Fig. 8. (a) Possible compositions of three components constitute ternary blend systems: (Right) D:A1:A2 and (Left) A:D1:D2. The elements include polymers (P), fullerene acceptors (FA), small molecules (SM), Non-fullerene acceptors (NFA), and dyes. Note: 2D materials and quantum dots can also be utilized as a third element. (b) Ternary system configurations: A:D1:D2 (top row) and D:A1:A2 (bottom row); and schematic of working mechanisms in Ternary OSC: Charge Transfer Model (a1, a2), Parallel Model (b1, b2), Alloy Model (c1, c2), and Energy transfer Model (d1, d2).

that the two donors may have combined to produce an alloy donor, enhancing active layer morphology and driving phase-separation [80]. The Chang-Zhi Li group synthesized a small-molecule (SM) donor BPR-SCL exhibiting a downshifted HOMO and high crystallinity. With the addition of BPR-SCL to the PM6:Y6 system, the molecular packing, charge mobilities, and exciton dissociation of the ternary blend significantly enhanced, yielding a PCE of 16.74% [115]. In 2019, Dai et al. developed ternary OSCs with a polymer donor and a small-molecule donor combination. As a third element, a medium bandgap small molecule donor TR was incorporated into a PTB7-Th: FOIC combination. The high crystallinity of TR controls the morphology of the blend films, which could improve the ordered packing of molecules and hole mobility in PTB7-Th. The best-performing device reached a remarkable PCE of 13.1% when the TR weight ratio in the ternary system was fixed at 25% [82]. J71 and PM6 can create an alloyed donor due to their

excellent compatibility, improving phase separation, and photon harvesting capability of active ternary layers. It was revealed that certain excitons on J71 can transport their energy to PM6 and then be dissociated at the PM6/Br-ITIC interface into the charge carriers. As a consequence, the modified ternary OSCs achieved a PCE of 14.13% while also improving J_{SC} (19.39 mA/cm²) and FF (78.4%) [116]. Li et al. used DRTB-T-C4, an extremely crystalline small molecule donor, as the guest material in a PM6:Y6 host mixture. The DRTB-T-C4 is orientated face-on, with an adequate coherence length of - stacking, in order to produce a highly ordered morphology and prevent material self-aggregation. The favorable positioning of DRTB-T-C4 at the PM6 and Y6 interface considerably contributed to optimizing the morphology. Incorporating a small molecule donor into the PM6: DRTB-T-C4:Y6 (1:0.15:1.2) TOSCs results in a very high PCE of 17.13% [83]. Due to their very similar chemical structures, the polymer donors

PM6 and S3 exhibit excellent compatibility, resulting in an alloy-like condition for the two donors in ternary blended films. The two donors' alloy-like composition is advantageous for improving film structure and donor energy level. Another polymer donor named S3 has a slightly lower HOMO level than PM6, enabling PM6:S3:Y6 based ternary OSCs to attain better V_{OC} than binary OSCs [84]. The addition of a polymer with a large bandgap ($E_g = 2.12$ eV), PB2F, to a PBDB-TF: BTP-eC9 mix resulted in a record efficiency of 18.6% [85]. Zhang et al. used blade coating to build ternary OSCs based on PBDB-T: PTB7-Th:FOIC blends. The crystallinity of FOIC was lowered when PTB7-Th was introduced to PBDB-T:FOIC blends because PTB7-Th and FOIC were more miscible than PBDB-T and FOIC, which revealed more improved charge transfer. Therefore, the optimized ternary device comprised of PBDBT:PTB7-Th:FOIC compositions (0.5: 0.5: 1) exhibited the highest PCE of 12.02% [86]. Zhu et al. constructed a ternary OSC by adding D18 into PM6:L8-BO blends. The combination of D18 with PM6 facilitates exciton diffusion, charge transport, and suppresses recombination. As a result, a record 19.3% efficiency was achieved. The ternary films' excellent molecular packing, effective phase separation, and expanded optical absorption range simultaneously enhanced the J_{SC} and FF [125].

2.3.2. Acceptor as a third component

Non-fullerene materials have become increasingly common in ternary blend OSCs in recent years. Their tunable molecular structure enables controlled broadening of the light absorption spectra and the potential to decrease the energy gap for charge transport, improving OSCs' optical and electrical properties. Different studies found that benzothiadiazole (BT)-based non-fullerene acceptors made an excellent choice for the third element of ternary organic solar cells. As the third element of the PM6:Y6 binary system, Chen's team announced the discovery of a novel non-fullerene acceptor named BTP-M in 2020. To enhance the LUMO energy level of the acceptor alloy, Y6 was combined with electron-donating methyl groups at the BTP-M terminals (Y6:BTP-M). Due to the acceptor alloy's higher LUMO energy level, the addition of 20% BTP-M with Y6 increased the V_{OC} from 0.844 to 0.875 V and decreased the E_{loss} from 0.49 to 0.45. Thus, the optimal ternary blend gadget registered the maximum PCE (17.03%) [87]. In many studies, IDT-based acceptors have been employed instead of fullerenes. As the third component in binary PM6:Y6 blends, Song et al. used 3TP3T-4F and 3TP3T-IC, two non-fullerenes small-molecule acceptors. The formation of energy cascades between PM6 and Y6 and the two visiting acceptors shows that they may facilitate charge transfer in ternary OSCs. It was found that 3TP3T-4F was more compatible with PM6 and Y6 than 3TP3T-IC. According to AFM studies, adding 3TP3T-4F made the ternary blend more likely to produce well-mixed phases without affecting its preferred morphology [117]. By combining a binary mixture of PBDB-TF:eC9 and HDO-4Cl, Bi et al. created a D:A1:A2 TOSC that behaves like an alloy. As a result, the LD switched from the pure eC9 acceptor phase (12.2 nm) to the HDO-4Cl:eC9 alloy phase (16.3 nm). When LD rises, there is less non-radiative recombination, so the $E_{loss-nonrad}$ ratio goes down. The alloy-like development of the two acceptors was favored, as shown by the phase separation morphology analysis. This, along with the lower $E_{loss-nonrad}$ that was designed by improving LD, led to the best record efficiency of 18.86% so far [118]. Based on a mixture of PM6:BO-4Cl:BTP-S2, Zhan et al. examined BHJ- and LbL-type ternary OPVs. As a result of its structure, BTP-asymmetric S2 is less miscible with PM6 than BO-4Cl. With LbL-type ternary OPVs, this could prevent unwanted donor-acceptor mixing during the LbL process, leading to an uniform phase distribution in which donors are enriched at the anode and acceptors are enriched at the cathode. Compared to BHJ-type ternary OPVs, creating well vertical phase distribution in LbL-type ternary OPVs reduced charge recombination while enhancing charge transport/collection capabilities, resulting in an improved FF of 78.04% and an increased J_{SC} of 27.14 mA cm^{-2} [119]. In order to create ternary OSCs, Tang and coworkers blended PM6:IT-4F with a

small-molecule acceptor N7IT. Adding N7IT to IT-4F reduced the PL intensity of IT-4F while increasing the PL intensity in the low-energy region. This revealed the pathway of energy from IT-4F to N7IT. In comparison to PM6:IT-4F, the crystal coherence length of the PM6: IT-4F:N7IT blend is shorter, leading to a higher electron mobility of $4.90 \times 10^{-4} \text{ cm}^2 \text{ V}^{-1} \text{ s}^{-1}$. As shown by AFM studies, the ternary blend possesses different nanofiber network structures with a RMS of 1.66 nm, showing that the acceptors of IT-4F and N7IT were highly morphologically compatible (Fig. 9) [120].

The non-fullerene acceptor IDIC, which has a structure comparable to Y6 but a higher energy level, was used by Li et al. to successfully increase the voltage in a ternary blended fullerene-free material. The results from AFM, GIWAXS, and TEM show that adding IDIC can lead to the formation of increased donor and acceptor phases while maintaining the homogenous fine film morphology and $\pi\pi$ stacking pattern of the original PM6:Y6. This is beneficial for improving charge mobilities and lowering monomolecular recombination. The PM6:Y6:IDIC system is then used to develop a ternary fullerene-free polymer solar cell with a 16.50% efficiency [121]. Liu et al. reported 14.25% efficiency utilizing ICBA: IT-4F as the acceptor and PM6 as the donor. PM6 crystallization is facilitated by the ICBA, which permits a portion of PM6 to split from the miscible IT-4F. As a result, an enrichment of IT-4F is seen at the surface, whereas PM6 accumulates underneath the active layer. Additionally, the increased crystallization of PM6 facilitates exciton separation and charge transfer, enhancing photovoltaic performance [122].

2.4. Tandem organic solar cells

The performance of single-junction OSCs is limited by several factors. First, single-junction OSCs are suffered from thermalization loss and transmission loss. When the energy of the excitons is greater than the bandgap of the active layer material, thermalization loss occurs. In contrast, transmission loss happens when photons with energies below the bandgap of the materials do not get absorbed in the active layer but pass through the active layer [127,128]. Second, poor charge mobility of organic semiconductors restricts the thickness of the active layer (~ 100 nm) and prevents adequate absorption, which limits OSCs to achieve high photocurrent. Third, even though the researcher's efforts to expand the absorption range by developing novel polymers and small molecules, the photocurrent generation is still constrained by the organic compounds' innate small absorption windows. These issues can be mitigated by combining two or more photoactive layers [129,130]. Under single sun irradiation, a single-junction OSC can convert just 30% of the solar energy; however, when two cells are employed in tandem, the conversion rate increases to 42% [128]. Therefore, tandem OSCs were utilized to increase solar energy collection and the PCE. The V_{OC} of a tandem OSC (consisting of two or more devices connected in series as sub-cells) is the sum of the V_{OC} of the individual sub-cells, whereas the J_{SC} is calculated from the sub-cell with the lowest J_{SC} . This shows that good efficiency in tandem OSCs depends on a balance between J_{SC} and V_{OC} for each sub-cell. Table 3 is an overview of the tandem OSC parameters discussed here. Tandem solar cells (TSCs) stack active layers with complementary band structures, which solves the thickness issue in single-junction cells and gives them a considerably larger range of spectral absorption [131,132]. Concurrently, the band structures of the active organic components in each sub-cell can be constructed and altered, thus limiting the thermal loss. These significant characteristics can theoretically be employed to predict a high-efficiency potential of up to 30%. TSCs combine wide bandgap and low bandgap materials with improving spectral coverage by tackling both absorption and thermal losses concurrently, thus increasing spectral coverage. Based on the sub-cell connection types and characteristics of the interconnecting layer (ICL), TSCs can be divided into parallel and series devices.

Fig. 10a depicts a 2-terminal (2T) monolithic polymer tandem device with matching band structures and compatible absorption spectra in two sub-cells. Both Fig. 10b and c represent the equivalent circuit of a series

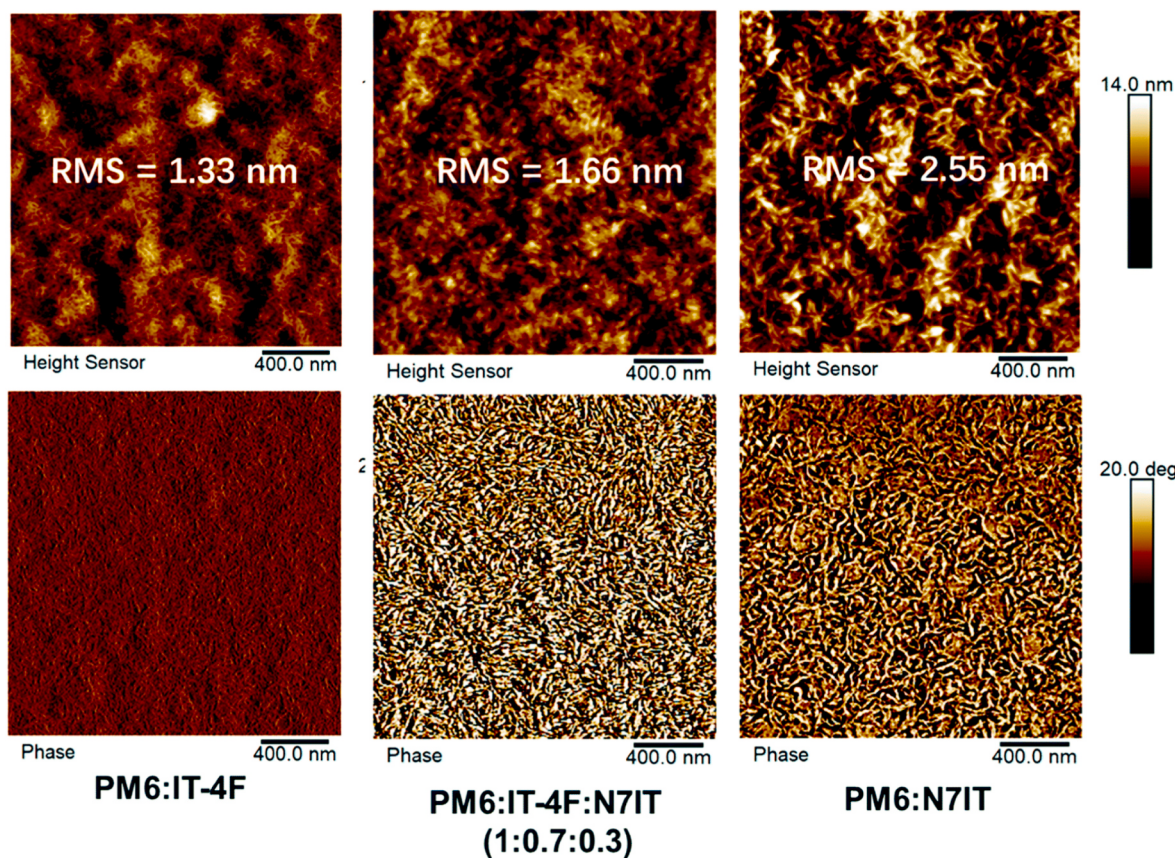


Fig. 9. Atomic force microscopy (AFM) height (top) and phase (bottom) images for the PM6:IT-4F:N7IT blend films. Reproduced with permission [120]. Copyright 2020, The Royal Society of Chemistry.

Table 3
List of photovoltaic performance of some tandem OSCs.

Front Cell	Rear Cell	ICL	J_{SC} (mA/cm ²)	V_{OC} (V)	FF (%)	PCE (%)	Ref.
PBDD4T-2F:PC ₇₁ BM	PBDTTT-E-T:IEICO	ZnO/PCP-Na	11.51	1.71	65	12.8	[134]
FTZA:IT-M	PTB7-Th:IEICO-4F	HSolar/ZnO NPs	14.6	1.64	67	16.1	[135]
PBDB-T-2F:PCD'TBT:IEICO-4F	PF3N-2TNDI/Ag/PEDOT:PSS	13.60	1.60	69	15.0	[136]	
PBDD4T-2F:PC ₆₁ BM	PBDD4T:PC ₇₁ BM	MoO ₃ /Ag/PFN	11.91	1.53	56	10.12	[137]
PBDB-T:F-M	PTB7-Th:O6T-4F:PC ₇₁ BM	M-PEDOT/ZnO	14.35	1.642	73.7	17.36	[13]
PM7:TffF-4Cl	PTB7-Th:COi8DFIC:PC ₇₁ BM	ZnO NPs:PEI/PEI/PEDOT:PSS	14.59	1.64	78	18.71	[138]
DTDCPB:C ₇₀	PCE-10:BT-CIC	BPhen: _{C60} /Ag/PEDOT:PSS	13.3	1.59	71	15.0	[139]
PTQ10:m-DTC-2Cl	PTB7-Th:BTPV-4F-eC9	MoO _x /M-PEDOT:PSS/ZnO NPs	14.65	1.621	70.20	16.67	[140]
PM6:SFT8-4F	PTB7-Th:BT-CIC:BEIT-4F	MoO ₃ /PEDOT:PSS/ZnO NPs	14.1	1.66	68	15.9	[17]
PBDB-TF:GS-ISO	PBDB-TF:BTP-eC9	e-TiO _{1.76} /PEDOT:PSS	13.14	2.01	76.75	20.27	[141]

arrangement of TSCs. The total open circuit voltage ($V_{OC} \approx V_{OC1} + V_{OC2}$) of a TSC is the sum of the voltages of its individual sub-cells, and the short current density (J_{SC}) of a TSC is bounded by the minimum J_{SC} of its sub-cells [133].

The homo tandem OSCs were developed by Liu et al. employing the small molecule SMPV1 as the donor. In order to provide an ohmic contact with low resistance between homo-tandem devices, PSS was utilized as the interconnection layer (ICL), which is a solution-processed conjugated polyelectrolyte (CPE) with a modified PEDOT bilayer structure. As a result, the homo-tandem OSCs' optical absorption was enhanced, enabling them to fully utilize all of the photon energy contained in their absorption spectrum with the aid of this superior ICL. The optimized tandem OSCs achieved a PCE of 10.1% with a V_{OC} of 1.82 V [142]. According to Meng et al., a structure that was solution-processed rather than vacuum-processed achieved an OSC record efficiency of 17.3% under AM1.5G light. A binary blend of PBDB-T:F-M and a ternary blend of PTB7-Th:O6T-4F:PC₇₁BM formed the active layers of the front

and rear sub-cells, respectively. These active layers were connected by an ICL made of PEDOT:PSS/ZnO. Based on their analysis of a semi-empirical model, they concluded that if the λ_{onset} of the rear cell is around 1100 nm and the average external quantum efficiency (EQE), photon energy loss (E_{loss}) and FF are all around 75%, then a PCE of 20% is achievable. The authors utilized the Small molecule COi8DFIC (also known as O6T-4F) based on the analysis, which nearly satisfies these parameters because it starts to absorb infrared light about 1050 nm. The resulting single-junction device blended with PTB7-Th as the donor and PC₇₁BM as the secondary acceptor showed high J_{SC} , FF (69.7%), EQE >70%, and low E_{loss} (0.51eV). The recent development of novel NFAs and the widely tunable band structure of these A-D-A configurations allowed for an optimal selection of rear cell material [13].

The use of NFAs in tandem with OSCs was further demonstrated by the rapid emergency response provided by effective NFAs. As an example, Cui et al. used a pair of NFAs with different bandgaps in tandem OSCs to increase the light absorption. The front sub-cell was

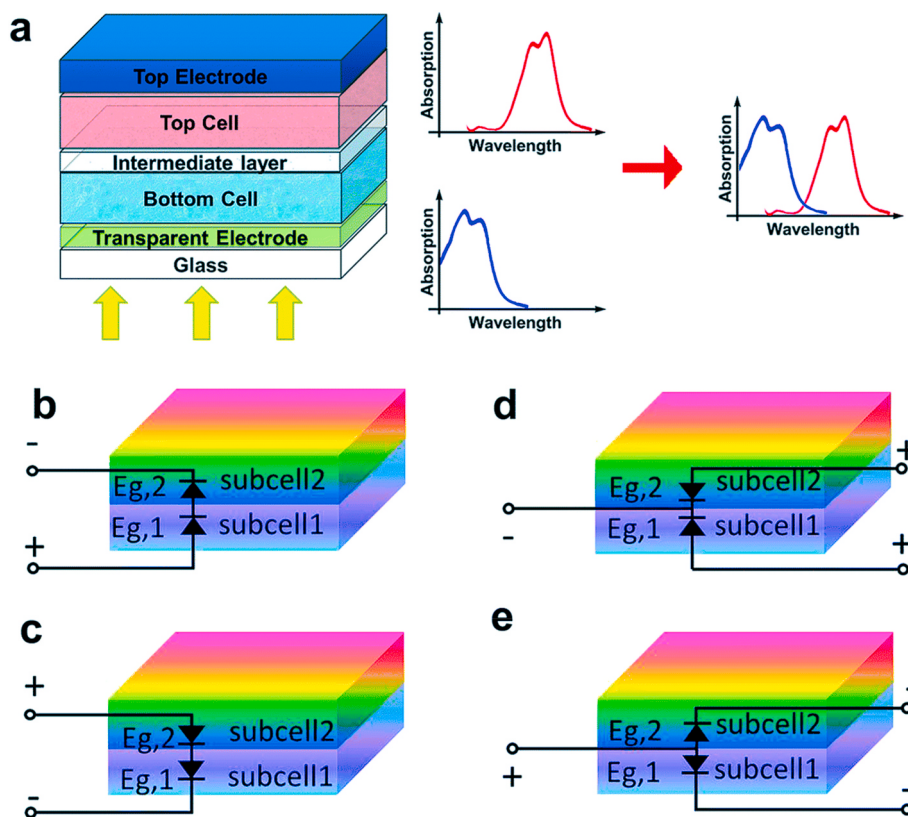


Fig. 10. Schematic of a polymer tandem device (a) with two sub-cells having different but complementary absorption spectra. A series connection of conventional (b) and inverted (c) tandem solar cells. Also, a parallel connection of conventional (d) and inverted (e) tandem solar cells. Reproduced with permission [133]. Copyright 2019, The Royal Society of Chemistry.

composed of ITCC-M:PBDB-T whereas the rear sub-cell was composed of PBDTTT-E:IEICO; hence, there was little power loss and complementary photo response spectra were obtained. In double-junction tandem OSCs, a PCE of 13.8% was attained with an ICL based on PCP-Na and ZnO NPs [131]. Ho and colleagues [135] constructed high-performance tandem OSCs by using HSolar/ZnO NPs as the ICL, PTB7-Th:IEICO-4F as a front sub-cell and FTAZ:IT-M as a rear sub-cell, respectively. The HSolar/ZnO NPs demonstrated improved charge extraction capabilities and favorable wettability on the sub-cell, allowing for the realisation of a tandem solar cell with a PCE of 14.7%. Additionally, Qin et al. demonstrated tandem OSCs processed entirely without the use of halogenated solvents. Polymer donors PTB7-Th and PTQ10 were combined with NFAs BTPV-4F-eC9 and *m*-DTC-2Cl to create complementary sub-cells. To demonstrate the potential for future large-scale manufacture, an OSC with a PCE of 16.67% was created through this process [140]. Zheng et al. recent work on tandem OSCs showed for the first time that the PCE was over 20%. As ICL, PEDOT:PSS and electron-beam evaporated TiO_x were utilized. As a result, PEDOT:PSS and electron-beam evaporated TiO_x exhibited a clean interface, suitable energy levels, excellent conductivity, and a low Schottky barrier. Likewise, the tandem OSC had an efficiency of 20.27% [141]. Wang and his group constructed tandem OSCs by introducing AITC small molecule acceptor into PBDB-TCl: BTP-eC9 active layer. PFBCPZ:AITC was employed as the bottom active layer and PBDB-TCl:AITC:BTP-eC9 was used as the top active layer in this tandem OSC. Including AITC into the active layer increased crystallinity and altered domain size, resulting in a record PCE of 20.6% and a higher open circuit voltage [143]. Combining a PM6:O1-Br based top active layer with a PTB7-Th:BTPSeV-4F based bottom active layer, the tandem organic solar cell achieves a 19% power conversion efficiency. With the addition of BTPSeV-4F, the photovoltaic performance of the tandem organic solar cells is enhanced by limiting the generation of triplet excitons and lowering energy losses [144].

3. Stability of organic solar cells

Organic solar cells are cheaper and flexible than their crystalline silicon counterparts, but they do not provide the same level of efficiency and stability compared to silicon solar cells. Silicon solar cells have an efficiency of around 26.6% [145], while the highest efficiency for organic photovoltaic reached 19% [7]. An OPV's performance must be stable across its lifetime for the technology to be commercially viable. Every new product utilized in large-scale energy generation must fulfil exceptionally high criteria because well-established PV manufacturers utilizing materials like crystalline silicon or cadmium telluride with warranty for 25 years [146]. Maintaining performance for 10 years, as is thought to be sufficient for OPVs to become economically competitive, is a significant challenge [147,148].

The instability of OSCs is influenced by various factors, as shown in Fig. 11, which have their different mechanisms of degradation. These factors can be divided into two categories: intrinsic and extrinsic factors, which are discussed in this section. External factors consist of oxygen, heat, moisture, light, mechanical stress, etc.

3.1. Intrinsic factors

The intrinsic instability factors of OSCs include three types: unstable morphology, unstable buffer layer, and diffusion of metal electrodes.

3.1.1. Unstable morphology

In the active layer, the phase distribution of donor and acceptor is categorized into three parts, i.e., acceptor-rich phase, donor-rich phase, and co-mixing phase of donor/acceptor [149,150]. Depending on the aging situation, the phase separation of acceptor and donor might vary because of the high mobility of organic materials. When OSCs come into contact with light illumination, thermal annealing, vapor, and oxygen in

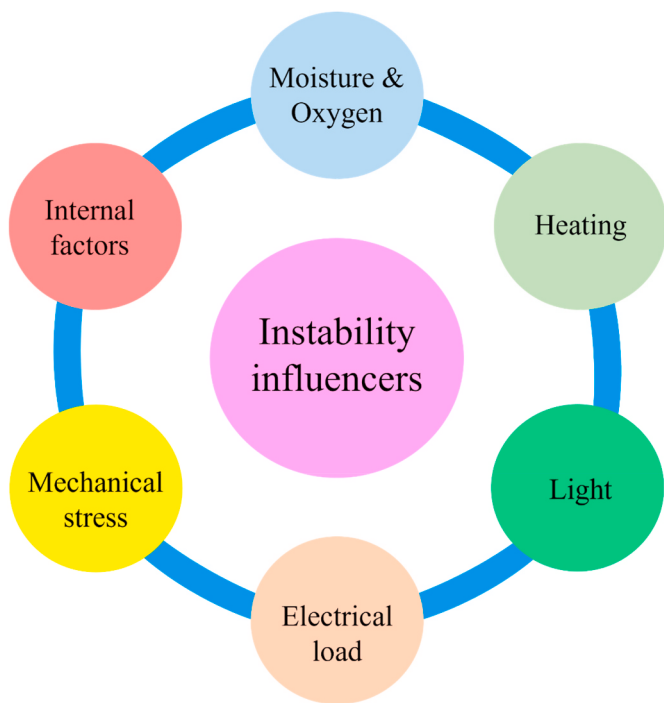


Fig. 11. Schematic of the mechanisms that cause OSCs to be unstable. Each of these parameters has an impact on the degradation of OSCs.

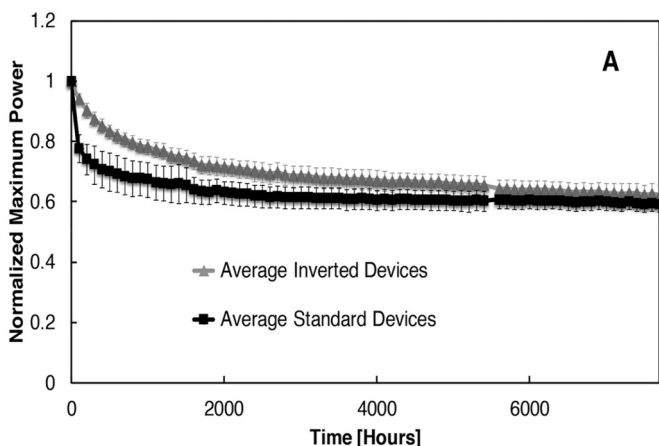


Fig. 12. The normalized maximum power of PCDTBT:PC₇₁BM solar cells aged in an environmental chamber is plotted against illumination time. Burn-in degradation reduces initial performance by nearly 40% over the first several thousand hours. Reproduced with permission [163]. Copyright 2015, American Chemical Society.

the air, the active layer's morphology is endangered. According to previous reports, when OPVs are encapsulated and stable in the dark, they degrade promptly in the first several hundred hours of illumination [151–153]. The initial span of abrupt degradation is typically referred to as "burn-in". Acute preliminary loss may occur; up to 40% burn-in loss is detected in PCDTBT solar cells [152,154,155], and in the case of PBDTTT-EFT solar cells, it is up to 60% [156] (see Fig. 12). Photon interactions with PCDTBT cells provide an explanation for burn-in losses. In the dark, the device is not degraded even when the device subjected to a current equal to that found in a short circuit [153]. The diffusion of Non-fullerene-acceptors (NFAs) is a major cause of morphological evolution which is reported recently by Ghasemi et al. [157]. The Y6-like NFAs show a large diffusivity at low glass transition temperature affecting the unstable morphology [158].

Sometimes, additive solvents with high boiling points are used in the photoactive mix to improve efficiency; in turn, these additives crucially decrease the device's stability [159–161]. Some additives are extremely photosensitive, allowing light to either directly saturate the polymer's conjugated backbone or be trapped by the fullerene moieties. They have the ability to accelerate the photooxidation of the bulk heterojunction layer [160,162].

3.1.2. Unstable buffer layer

The advent of the buffer layer has been shown to achieve success in enhancing PCE due to the fact the higher strength degree alignment is ideal for charge transport and extraction. The effective physics of the Cathode buffer layer (CBL) with corresponding electronic phenomena at the CBL/photoactive layer interface upon the structural and chemical parameters are described in a recent review [164]. Besides, properties such as acidity and hydrophilicity of the buffer layer greatly influence the stability of the OSC. The conventional OSC containing PEDOT:PSS layer was very unstable because both the PCE and J_{sc} were reduced to less than half of its starting value after storing for 50 h [165]. It was observed by Meng et al. that the acid PEDOT:PSS etched the ITO electrode, causing a quicker degradation compared to the neutral ones [166]. In general, the effect of acid etching on a device can be expressed in the following two ways. Inferior charge transport property occurs by the recombination centres (indium and tin ions). These ions can flow into the bulk-heterojunction, affecting both charge separation and charge transport in the photoactive layer. Contrarily, the work function of ITO may be irreversibly altered due to the chemical reaction with the buffer layer, resulting in poor device stability [167]. ZnO is employed as the electron transport layer (ETL) in inverted OSCs that have an innate photocatalytic UV response. The active OSC layers are subsequently damaged when exposed to light. The photo-stability of the NFA-OSC on the ZnO interlayer was studied by Son et al., who reported that the ITIC-based POSCs have poor photo-stability. The vinyl group in ITIC is chemically more sensitive than the stable aromatic units in the organic active components, leading to the compound's poor stability. Severe burn-in degradation and decreased FF and V_{OC} under illumination arise from the decomposition of ITIC, which degrades the electron transport capabilities of the active materials near ZnO [168].

3.1.3. The diffusion of metal electrodes

Using cross-sectional TEM technology, it analyzed the long-term stability of OSCs and found that silver diffusion caused irregularities in the J-V curve after a particular time period [169]. When PEDOT:PSS is in contact with an ITO anode, it quickly corrodes the surface of ITO due to its acidic and hygroscopic properties. Because of this, indium diffuses into the active layer, trapping charge carriers [170]. Al is usually used as a cathode because it is easy to oxidize into Al_2O_3 . Water can penetrate the bottom layer via pinholes and voids, which makes the device unstable. An investigation by Voroshazi et al. showed the diffusion of the Al electrode affects the instability of OSCs [171].

3.2. External factors

Extrinsic degradation happens with ambient conditions such as the aging of OPVs, in the dark condition or optical illumination, and the intrusion of oxygen and vapor into the device.

3.2.1. Oxygen in OSCs

Oxygen plays a major role in extrinsic degradation (Fig. 13) in OSCs due to the factors described below. Firstly, fullerene is nonreactive with water, and in the presence of fullerene, Aluminum can act as a passivating agent against water-induced corrosion [172]. Besides, electron-transport properties may suffer much while exposed to oxygen in the environment [173]. Also, surface dipoles can form by raising the work function of metal with oxygen [174]. Seemann et al. evaluated the photoactive layer of the cell is the location of degradation

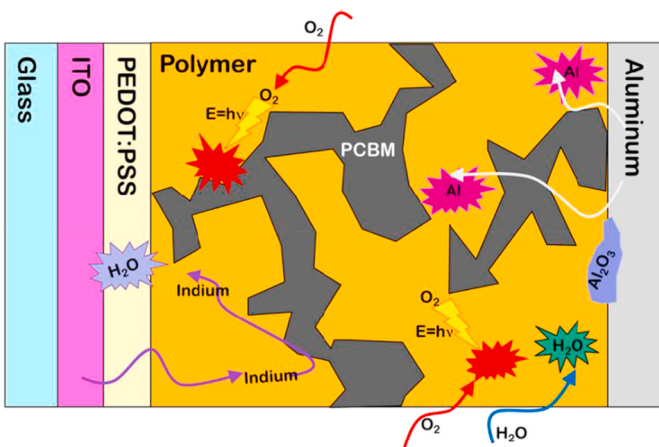


Fig. 13. Schematic illustration of degradation mechanism of OSCs with oxygen and water. This figure has been used from Ref. [181] is licenced under CC BY 4.0.

semi-transparent P3HT:PCBM solar cells with high conductivity PEDOT:PSS top electrodes [175]. Norrman et al., observed that the top PEDOT:PSS layer resists air penetration more effectively than the aluminium cathodes in conventional OSCs from their synthesized OSCs with a structure of ITO/ZnO/PCBM:P3HT/PEDOT:PSS/Ag [176]. An inverted hybrid solar cell was fabricated by another group with ITO/oxides/MEH-PPV/Ag structure. They found that the application of ZnO, or TiO₂, or Nb₂O₅, requires the presence of oxygen for the actual functioning of these oxides as electron acceptors. Those hybrid solar cells may unstable abruptly under light irradiation in free space, although they can partially be recovered upon exposure to air [177]. Andreasen et al. investigated the time-dependent oxygen concentration in OSCs and reported that oxygen assembles in the active layers, which is linearly time-dependent, causing instability [178]. Airborne oxygen reacts with NFAs in the active layer, causing damage to the conjugated structures via photooxidation [179]. However, even in the absence of illumination, penetrative oxygen in active layer films can influence the molecular structure of organic semiconductors. To investigate the stability of NFA-based OSCs, Fahlman et al. utilized three ladder NFAs (*o*-IDTBR and *p*/m-ITIC). Since the changed energy level can affect the energy alignment between the NFA and donor in the active layer, indicating a strong reaction between NFAs and oxygen and leading to a drop in the PCE [180].

3.2.2. Moisture induced degradation

The intrusion of water in the device is one of the critical limiting factors in device stability (Fig. 13). Water may diffuse through the device by the medium of the PEDOT:PSS buffer layer and metal electrodes having an amount of 42 kJ mol⁻¹ activation energy which is found using Arrhenius relation [182]. As water is an oxidation agent, it can harm low work-function metal electrodes such as Al. For instance, severe defects were found in the case of Al electrode [183,184], which can fasten up water ingress [185]. Besides, the appearance of water into the active layer interface and hence an insulating metal oxide interlayer can be formed by the electrode, which in turn causes a decrement of the effective active layer or electrode interface area, resulting in harm to charge extraction [186]. Finally, if water molecules diffuse into the active layer, they can displace PC₆₁BM and cause excessive fullerene aggregation. A harmful effect on exciton dissociation is associated with the extensive decrement of phase separation at D/A interfaces and is responsible for a considerable reduction in device performance [187].

3.2.3. Optical illumination

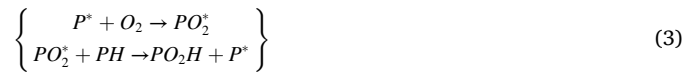
As a solar cell is a device that converts light into electricity, it must be operated under light. But most of the OSCs show instability upon optical

illumination. PCE is half after 22 h illumination in the case of MDMO-PPV/PC₆₁BM-based solar cells [188]. Another report shows for another two prototypical systems that upon illumination for 500 h, the PCE of P3HT/PC₆₁BM decreased from 3.4% to 1.9% and 5.7%–3.8% for PCDTBT/PC₇₁BM [189]. Generally, photodegradation includes two mechanisms, i.e., photochemical degradation and photophysical degradation. The photochemical degradation that causes photooxidation is generally attained through a free-radical reaction [190]. There are three parts consisting of initiation, propagation, and termination, which are depicted in Equations (2)–(5). In general, the first step (initiation) causes a breaking of the bond. After forming a free radical, the propagation is started through the film by either diffusion or reaction. The direct mechanism behind absorption loss is the scission of the conjugated bonds, which arises at the time of propagation. Lastly, the recombination of two free radicals results in termination.

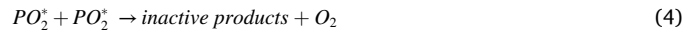
Initiation



propagation



termination



branching



On the other hand, photophysical degradation is another major cause of photodegradation. An acute problem related to the photophysical effect on OPV performance is photoinduced charge accumulation, reported by some authors [191,192]. Accumulation of electrons and holes in two trap sites, as well as the energy diagram of bulk heterojunction OSC's are illustrated in Fig. 14a and b. Dennler et al. reported the dependence of V_{OC} on the difference between the HOMO level of the donor and the LUMO level of the acceptor for the reason of ohmic contacts on both interfaces of the active layer/anode or cathode [193]. The mitigation of the energy band slope is appeared after 8 h of light exposure because of the accumulation of electrons and holes in the two trap sites, yielding a reduction of V_{OC} (Fig. 14c).

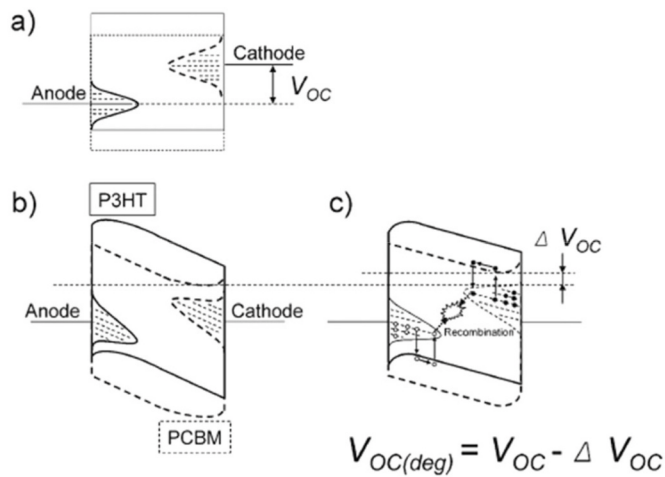


Fig. 14. Diagram illustrates the bulk heterojunction organic solar cell under (a) initial open circuit circumstances (V_{OC}), (b) initial short circuit conditions (J_{SC}), and (c) after degradation. Carriers, or holes (open circle) and electrons (filled circle), are concentrated in two trap sites (dashed line). Reproduced with permission [192]. Copyright 2009, John Wiley and Sons.

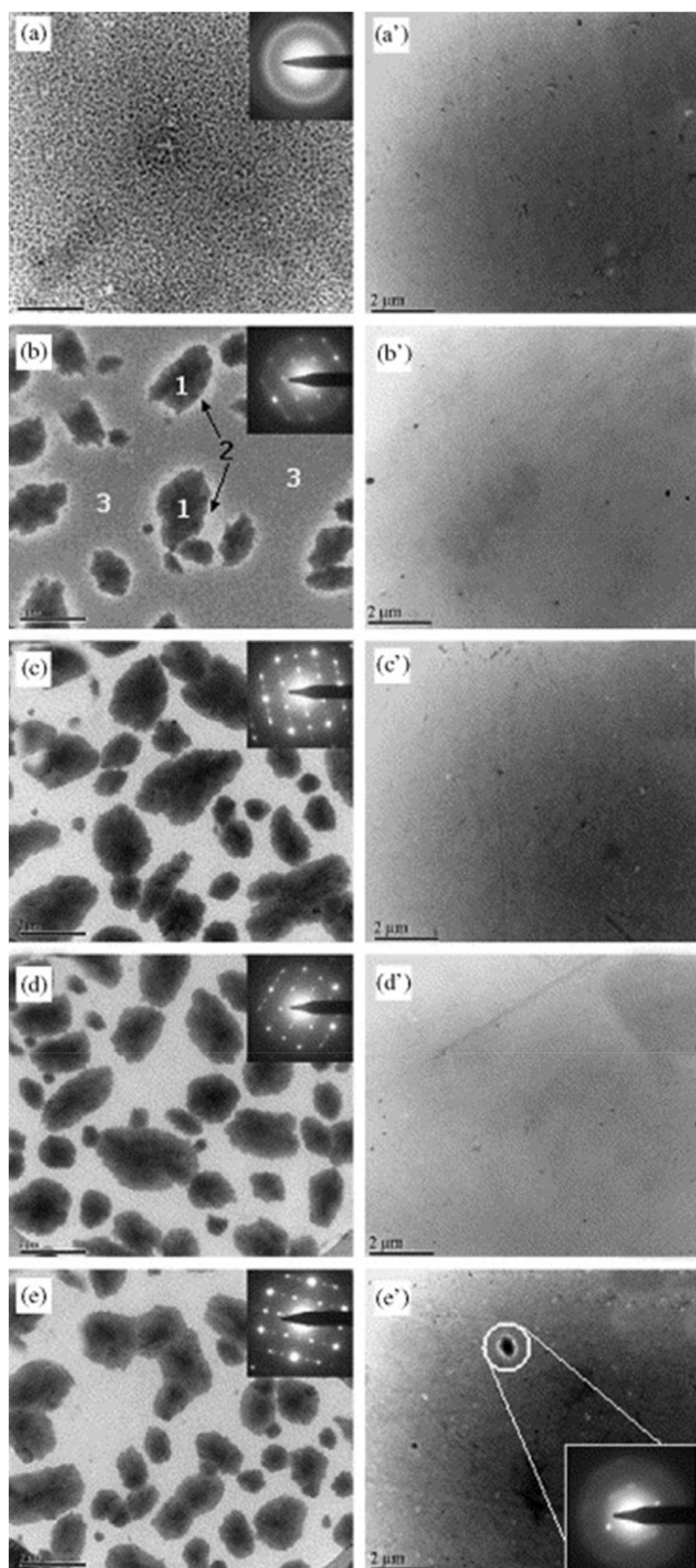


Fig. 15. TEM images of OSC containing MDMO-PPV:PCBM (1:4) based active layer (a–e) and 'high T_g PPV:PCBM (1:4) based active layer (a'–e'). The solar cells were heated at 110 °C for the following periods of time: 0 h (a, a'), 1 h (b, b'), 2 h (c, c'), 4 h (d, d'), and 16 h (e, e'). This resulted in the creation of huge PCBM-clusters for the MDMO-PPV based active layers while keeping a more stable morphology for the 'high T_g PPV' based active layers (scale bar: 2 μm). Reproduced with permission [207]. Copyright 2007, Elsevier.

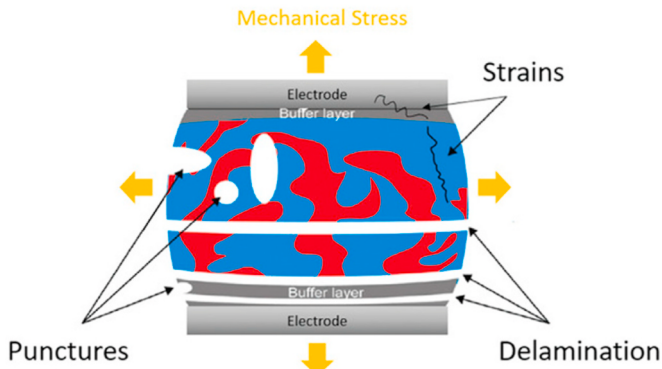


Fig. 16. Illustration of how mechanical stress, like punctures, strains, and delamination, can cause mechanical damage. Reproduced with permission [215]. Copyright 2020, John Wiley and Sons.

3.2.4. Temperature effect

Solar cells convert light energy into electricity; hence it is necessary to expose the solar cell to the sun, which causes heating through radiation. The main cause of instability is that solar cells have a high working temperature that is significantly lower than the decomposition temperature of the materials in the photoactive layer [194–196]. In the case of the active layer, the ideal morphological state is typically out of thermodynamic equilibrium [197,198]. Nonetheless, even in the absence of extrinsic factors, that morphology can gradually achieve equilibrium. According to reports, heating is responsible for the increased thermodynamic energy needed to accelerate the equilibrium case [199–201] (see Fig. 15). Researchers Greenbank et al. looked at how different hole transport layers and metal electrode pairs affected OSCs' thermal stability, finding that devices using silver and MoO₃ as an electrode and the hole transport layer material, respectively, performed the worst. In contrast, WO₃ acted as the hole transport layer and Al as the top electrode resulting in better thermal stability [202]. Wang et al. found that between 100 and 145 °C, the morphology of a PCDTBT/PC₇₁BM (1:4) film hardly changed, whereas coarse phase separation took place in the film at the time of annealing at a temperature higher than 155 °C [203]. Two types of behaviour, such as aggregation or crystallization of PCBM were observed with different thermal annealing times [204]. The authors found that both the size and number of aggregated fullerene clusters had a proportional relationship with time, causing a decrement in D-A interfaces, leading to lower PCE. Farooq et al. showed that the efficiency rate of a thin-film OSC depreciates by 0.32% from numerical modelling [205]. Yang et al. studied PM6:BTBT-2Cl-based devices operating at high temperatures for various periods of time. The morphology is changed by the creation of large crystals after a 24-h thermal annealing process. The heat treatment-induced morphological change lowers exciton dissociation as well as OSC efficiency [206].

3.2.5. Mechanical stress

Mechanical stability is indispensable for the performance of OSCs in the environment. So, it is crucial to study the roll-to-roll (R2R) manufacturing and the operational stability of OSCs, particularly for exterior applications [208]. Dupont et al. [209] described the important aspects of inter-layer adhesion in the case R2R processed OSCs. However, it is essential to address the mechanism behind mechanical degradation. For instance, delamination of the active layer, buffer layers, also electrode layers can be affected by mechanical stress. Because delamination depends on the adhesion energy of each of the layers, endangering the charge transport and extraction. It was reported that mechanical stress could damage the polymer-fullerene layer, electrodes, interfacial layers, and interfaces [210]. Some other phenomena, namely cracking, scratches, punctures, and bends, can occur in the

earth's atmosphere [211]. At a maximum strain of 14%, OSCs maintained 90% of their initial PCE, and electrode cracking will occur at greater strains, demonstrating that tensile strain can initiate the nanostructure transformation of the photoactive layer [212]. Furthermore, punctures and edge delamination play catalytic roles in oxygen and moisture-induced degradation [213]. Awartani et al. [214] used P3HT:PCBM based blend and found increasing elastic modulus with decreasing crack onset strain of the BHJ photoactive layer (see Fig. 16).

3.3. Strategies in improving the stability of OSCs

It is essential for an OSC to operate successfully that the device be both internally and extrinsically stable. oxidative, mechanical, thermal, irradiation, and photochemical instabilities must be sustained by the OSC modules. Numerous solutions have been implemented to overcome the stability challenges inherent in an OSC's operating duration. Inverted geometry helps to boost stability. There are many approaches to enhance the stability of OSCs, such as the use of inverted geometry and alternative electrodes, optimization of ETL and HTL, morphology control, encapsulation, etc [216–220]. Regardless of whether an OSC has a conventional or non-conventional geometry, the exposed surface of the active layer (without ITO shielding) will always have a low work-function (WF) cathode that is vulnerable to both water and oxygen. To solve the poor air stability of conventional OSCs, inverted geometry was created in which the position of the anode and cathode are switched [216,221–223]. Zhu et al. examined the stability of OSCs using a variety of various structural configurations. After being exposed to the air for 50 days, the inverted structure of the PBDB-T:ITIC-based devices kept only 2.4% of its initial PCE, whereas the conventional devices retained roughly 58%. Standard devices degrade with time because to the reaction of PEDOT:PSS with ITIC, which reduces the built-in potential [224]. For OSCs, it is critical to optimise the electron transport layer (HTL) and hole transport layer (HTL). The most popular HTL material, PEDOT:PSS, is also the most detrimental to devices because to its acidic and hygroscopic properties. The underlying ITO is corroded with time, allowing more diffusion into the photoactive layer. Therefore, certain additional materials have been reported to function as HTLs in OSCs. The most thoroughly studied non-acidic PEDOT:PSS alternatives are metal oxide-based HTLs [223,225]. The solution-processed MoO₃ was found to be superior than PEDOT:PSS in a number of different OSC systems, proving its versatility and applicability [226]. Lithium fluoride (LiF), as well as Ca and ZnO, are the most often utilized ETLs in normal and inverted geometry, respectively. These materials are unstable in the ambient environment due to their reactivity with oxygen, water, air, and light. To significantly improve the stability, metal oxides, electron transport polymers, stable metals, and modified ZnO can be employed in place of LiF, Ca, and ZnO. Furthermore, there are a number of ways in which ZnO can be modified to overcome the stability issues of a single ZnO ETL. Improving ZnO's electron transport characteristics with the addition of metal dopants is a common practise [210,227–229]. Zhou et al. modified ZnO nanoparticles in the precursor solution with poly[(9,9-bis((N,N-dimethyl)-N-ethylammonium)-propyl)-2,7-fluorene]-alt-2,7-(9,9-diocetylfluorene)] dibromide(PFN-Br), which improved the performance and stability of the devices as a whole. The PCE of modified devices was 90% preserved after a month, while that of unmodified devices was 80% [228]. The morphology of the active layer has a significant impact on OSC stability. The morphology of the active layer can be improved in a number of approaches to increase device stability, such as by the selection and modification of acceptor/donor materials, optimization of processing conditions (e.g., solvent optimization, thermal annealing), the addition of a third component, etc [219,230–233]. Using a chlorination method in PBDB-TF polymer donor, Son et al. synthesized a novel polymer donor called PBDB-TSCI. The efficiency of the PBDB-TF solar cell device dropped to 75% after annealing for 34 h, while the efficiency of the PBDB-TSCI remained rather stable, dropping down only 5%. These findings showed the benefit and the impact of the

chlorination treatment for improving OSC stability [230]. Yao et al. developed a family of volatile monomers which contain the IT-4F end-group's chemical structure. Among these monomers the SA-1 monomer exhibited the best performance as a solid additive. The PCE of the SA-1 doped PBDB-TF:IT-4F-based devices reported 13.8%, while the PCE of undoped devices was 12.2%. The doped devices were more stable in both thermal and storage conditions than the unmodified ones [219]. Encapsulation is a well-established strategy used by solar cell manufacturers to increase the device's stability. Elkington et al. encapsulated BHJ OSCs with a bisphenol A-based epoxy resin. The encapsulant is proven to be an effective barrier against airborne degradation [234].

4. Conclusion

OSCs have achieved remarkable scientific development in the previous few years because of attempts to design high-performance photovoltaic materials. The PCE improvement of OSCs has been significantly aided by advances in solar material technology. In order to create OSCs with performance characteristics more than 10% PCE and even 19%, a variety of innovative materials have been developed. A high PCE performance necessitates both the acceptor's and donor's complementary absorption to get the most out of the photons and hence generate a large current flow. It's also important to make sure that the energy levels of the acceptors and donors are a good match. HOMO of the polymer donor and LUMO of the non-fullerene acceptors must be carefully selected to optimise Voc and provide a strong driving force for charge creation and transport. Even though efficient fullerene-free OSCs have energy losses as low as 0.5 eV (or even lower), research into new photovoltaic materials with reduced energy losses is still desired. For high performance OSCs, the preferred blend morphology is also crucial. Exciton separation is favored by domains of appropriate size, high purity, and outstanding charge mobility. In addition, the vertical charge transfer is facilitated by a film morphology with a desired face-on orientation. Prior to commercialising OSCs, the long-term viability of those systems must be ensured. As a result of the many things that have been done to make devices more stable, like adding additives and interfacial layers and encapsulating them. The morphological and chemical stability of NFAs against numerous factors, including as oxygen, heat, water, and light, still has to be enhanced by modifying their molecular structure, even though it has been demonstrated that OSCs are stable against stresses from the heat, air, and light.

CRediT authorship contribution statement

Walia Binte Tarique: Writing – review & editing, Writing – original draft, Data curation. **Ashraf Uddin:** Writing – review & editing, Supervision, Conceptualization.

Declaration of competing interest

The authors declare that they have no known competing financial interests or personal relationships that could have appeared to influence the work reported in this paper.

Data availability

The authors do not have permission to share data.

Acknowledgements

The authors would like to express their gratitude to the OPV research group, the staffs of the Photovoltaic and Renewable Energy Engineering School (SPREE), UNSW.

References

- [1] O. Inganäs, Organic photovoltaics over three decades, *Adv. Mater.* 30 (2018), 1800388, <https://doi.org/10.1002/adma.201800388>.
- [2] K.A. Mazzio, C.K. Luscombe, The future of organic photovoltaics, *Chem. Soc. Rev.* 44 (2014) 78–90, <https://doi.org/10.1039/C4CS00227J>.
- [3] C. Liu, C. Xiao, C. Xie, W. Li, Flexible organic solar cells: materials, large-area fabrication techniques and potential applications, *Nano Energy* 89 (2021), 106399, <https://doi.org/10.1016/j.nanoen.2021.106399>.
- [4] L. Hong, H. Yao, Y. Cui, P. Bi, T. Zhang, Y. Cheng, Y. Zu, J. Qin, R. Yu, Z. Ge, J. Hou, 5% efficiency organic solar cells with a hybrid planar/bulk heterojunction, *Adv. Mater.* 33 (2021), 2103091, <https://doi.org/10.1002/adma.202103091>, 18.
- [5] J. Qin, L. Zhang, C. Zuo, Z. Xiao, Y. Yuan, S. Yang, F. Hao, M. Cheng, K. Sun, Q. Bao, Z. Bin, Z. Jin, L. Ding, A chlorinated copolymer donor demonstrates a 18.13% power conversion efficiency, *J. Semicond.* 42 (2021), <https://doi.org/10.1088/1674-4926/42/1/010501>, 010501–5.
- [6] X. Xu, L. Yu, H. Meng, L. Dai, H. Yan, R. Li, Q. Peng, Polymer solar cells with 18.74% efficiency: from bulk heterojunction to interdigitated bulk heterojunction, *Adv. Funct. Mater.* 32 (2022), 2108797, <https://doi.org/10.1002/adfm.202108797>.
- [7] Y. Cui, Y. Xu, H. Yao, P. Bi, L. Hong, J. Zhang, Y. Zu, T. Zhang, J. Qin, J. Ren, Z. Chen, C. He, X. Hao, Z. Wei, J. Hou, Single-junction organic photovoltaic cell with 19% efficiency, *Adv. Mater.* 33 (2021), 2102420, <https://doi.org/10.1002/adma.202102420>.
- [8] H. Kallmann, M. Pope, Photovoltaic effect in organic crystals, *J. Chem. Phys.* 30 (1959) 585–586, <https://doi.org/10.1063/1.1729992>.
- [9] R.N. Marks, J.J.M. Halls, D.D.C. Bradley, R.H. Friend, A.B. Holmes, The photovoltaic response in poly(p-phenylene vinylene) thin-film devices, *J. Phys. Condens. Matter* 6 (1994) 1379, <https://doi.org/10.1088/0953-8984/6/7/009>.
- [10] C.W. Tang, Two-layer organic photovoltaic cell, *Appl. Phys. Lett.* 48 (1986) 183–185, <https://doi.org/10.1063/1.196937>.
- [11] G. Yu, J. Gao, J.C. Hummelen, F. Wudl, A.J. Heeger, Polymer photovoltaic cells: enhanced efficiencies via a network of internal donor-acceptor heterojunctions, *Science* 270 (1995) 1789–1791, <https://doi.org/10.1126/science.270.5243.1789>.
- [12] J. Fu, P.W.K. Fong, H. Liu, C.-S. Huang, X. Lu, S. Lu, M. Abdelsamie, T. Kodalle, C. M. Sutter-Fella, Y. Yang, G. Li, 19.31% binary organic solar cell and low non-radiative recombination enabled by non-monotonic intermediate state transition, *Nat. Commun.* 14 (2023) 1760, <https://doi.org/10.1038/s41467-023-37526-5>.
- [13] L. Meng, Y. Zhang, X. Wan, C. Li, X. Zhang, Y. Wang, X. Ke, Z. Xiao, L. Ding, R. Xia, H.-L. Yip, Y. Cao, Y. Chen, Organic and solution-processed tandem solar cells with 17.3% efficiency, *Science* 361 (2018) 1094–1098, <https://doi.org/10.1126/science.aat2612>.
- [14] X. Xu, Y. Li, Q. Peng, Recent advances in morphology optimizations towards highly efficient ternary organic solar cells, *Nano Select* 1 (2020) 30–58, <https://doi.org/10.1002/nano.202000012>.
- [15] X. Guo, D. Li, Y. Zhang, M. Jan, J. Xu, Z. Wang, B. Li, S. Xiong, Y. Li, F. Liu, J. Tang, C. Duan, M. Fahlman, Q. Bao, Understanding the effect of N2200 on performance of J71: ITIC bulk heterojunction in ternary non-fullerene solar cells, *Org. Electron.* 71 (2019) 65–71, <https://doi.org/10.1016/j.orgel.2019.05.004>.
- [16] Z. Hu, F. Zhang, Q. An, M. Zhang, X. Ma, J. Wang, J. Zhang, J. Wang, Ternary nonfullerene polymer solar cells with a power conversion efficiency of 11.6% by inheriting the advantages of binary cells, *ACS Energy Lett.* 3 (2018) 555–561, <https://doi.org/10.1021/acsenergylett.8b00100>.
- [17] X. Huang, B. Sun, Y. Li, C. Jiang, D. Fan, J. Fan, S.R. Forrest, 15.9% organic tandem solar cell with extended near-infrared absorption, *Appl. Phys. Lett.* 116 (2020), 153501, <https://doi.org/10.1063/5.0005172>.
- [18] H.-L. Yip, A.K.-Y. Jen, Recent advances in solution-processed interfacial materials for efficient and stable polymer solar cells, *Energy Environ. Sci.* 5 (2012) 5994–6011, <https://doi.org/10.1039/C2EE02806A>.
- [19] Y. Wu, H. Bai, Z. Wang, P. Cheng, S. Zhu, Y. Wang, W. Ma, X. Zhan, A planar electron acceptor for efficient polymer solar cells, *Energy Environ. Sci.* 8 (2015) 3215–3221, <https://doi.org/10.1039/C5EE02477C>.
- [20] R. Sorrentino, E. Kozma, S. Luzzati, R. Po, Interlayers for non-fullerene based polymer solar cells: distinctive features and challenges, *Energy Environ. Sci.* 14 (2021) 180–223, <https://doi.org/10.1039/D0EE02503H>.
- [21] Y. Lin, J. Wang, Z.-G. Zhang, H. Bai, Y. Li, D. Zhu, X. Zhan, An electron acceptor challenging fullerenes for efficient polymer solar cells, *Adv. Mater.* 27 (2015) 1170–1174, <https://doi.org/10.1002/adma.201404317>.
- [22] P. Li, Z.-H. Lu, Interface engineering in organic electronics: energy-level alignment and charge transport, *Small Science* 1 (2021), 2000015, <https://doi.org/10.1002/smss.202000015>.
- [23] H. Zhang, Y. Li, X. Zhang, Y. Zhang, H. Zhou, Role of interface properties in organic solar cells: from substrate engineering to bulk-heterojunction interfacial morphology, *Mater. Chem. Front.* 4 (2020) 2863–2880, <https://doi.org/10.1039/DQQM00398K>.
- [24] C. Deibel, V. Dyakonov, Polymer–fullerene bulk heterojunction solar cells, *Rep. Prog. Phys.* 73 (2010), 096401, <https://doi.org/10.1088/0034-4885/73/9/096401>.
- [25] A.C. Mayer, S.R. Scully, B.E. Hardin, M.W. Rowell, M.D. McGehee, Polymer-based solar cells, *Mater. Today* 10 (2007) 28–33, [https://doi.org/10.1016/S1369-7021\(07\)70276-6](https://doi.org/10.1016/S1369-7021(07)70276-6).
- [26] M. Rita Narayan, J. Singh, Study of the mechanism and rate of exciton dissociation at the donor-acceptor interface in bulk-heterojunction organic solar cells, *J. Appl. Phys.* 114 (2013), 073510, <https://doi.org/10.1063/1.4818813>.

- [27] P. Cusumano, C. Arnone, M.A. Giambra, A. Parisi, Donor/acceptor heterojunction organic solar cells, *Electronics* 9 (2020) 70, <https://doi.org/10.3390/electronics9010070>.
- [28] P.K. Nayak, Exciton binding energy in small organic conjugated molecule, *Synth. Met.* 174 (2013) 42–45, <https://doi.org/10.1016/j.synthmet.2013.04.010>.
- [29] I.C. Ghosekar, G.C. Patil, Review on performance analysis of P3HT:PCBM-based bulk heterojunction organic solar cells, *Semicond. Sci. Technol.* 36 (2021), 045005, <https://doi.org/10.1088/1361-6641/abe21b>.
- [30] S.D. Dimitrov, J.R. Durrant, Materials design considerations for charge generation in organic solar cells, *Chem. Mater.* 26 (2014) 616–630, <https://doi.org/10.1021/cm402403z>.
- [31] T.F. Hinrichsen, C.C.S. Chan, C. Ma, D. Paleček, A. Gillett, S. Chen, X. Zou, G. Zhang, H.-L. Yip, K.S. Wong, R.H. Friend, H. Yan, A. Rao, P.C.Y. Chow, Long-lived and disorder-free charge transfer states enable endothermic charge separation in efficient non-fullerene organic solar cells, *Nat. Commun.* 11 (2020) 5617, <https://doi.org/10.1038/s41467-020-19332-5>.
- [32] J. Singh, M. Narayan, D. Ompong, F. Zhu, Dissociation of charge transfer excitons at the donor–acceptor interface in bulk heterojunction organic solar cells, *J. Mater. Sci. Mater. Electron.* 28 (2017), <https://doi.org/10.1007/s10854-017-6443-3>.
- [33] M. Narayan, J. Singh, Study of the mechanism and rate of exciton dissociation at the donor–acceptor interface in bulk-heterojunction organic solar cells, *J. Appl. Phys.* 114 (2013), <https://doi.org/10.1063/1.4818813>, 073510–073510–7.
- [34] X. Zhang, X. Zuo, S. Xie, J. Yuan, H. Zhou, Y. Zhang, Understanding charge transport and recombination losses in high performance polymer solar cells with non-fullerene acceptors, *J. Mater. Chem. A* 5 (2017) 17230–17239, <https://doi.org/10.1039/C7TA05865A>.
- [35] M.C. Schärber, N.S. Sariciftci, Efficiency of bulk-heterojunction organic solar cells, *Prog. Polym. Sci.* 38 (2013) 1929–1940, <https://doi.org/10.1016/j.progpolymsci.2013.05.001>.
- [36] M.R. Narayan, J. Singh, Effect of simultaneous excitation of singlet and triplet excitons on the operation of organic solar cells, *J. Appl. Phys.* 114 (2013), 154515, <https://doi.org/10.1063/1.4826199>.
- [37] J. Nelson, The Physics of Solar Cells, PUBLISHED BY IMPERIAL COLLEGE PRESS AND DISTRIBUTED BY WORLD SCIENTIFIC PUBLISHING CO., 2003, <https://doi.org/10.1142/p276>.
- [38] Physics of Solar Cells: From Basic Principles to Advanced Concepts, third ed. | Wiley, Wiley.Com. (n.d.). <https://www.wiley.com/en-us/Physics+of+Solar+Cells%3A+From+Basic+Principles+to+Advanced+Concepts%2C+3rd+Edition-p-9783527413126> (accessed October 9, 2022).
- [39] W. Ma, C. Yang, X. Gong, K. Lee, A.J. Heeger, Thermally stable, efficient polymer solar cells with nanoscale control of the interpenetrating network morphology, *Adv. Funct. Mater.* 15 (2005) 1617–1622, <https://doi.org/10.1002/adfm.200500211>.
- [40] M. Mohan, V. Nandal, S. Paramadam, K.P. Reddy, S. Ramkumar, S. Agarwal, C. S. Gopinath, P.R. Nair, M.A.G. Namboothiry, Efficient organic photovoltaics with improved charge extraction and high short-circuit current, *J. Phys. Chem. C* 121 (2017) 5523–5530, <https://doi.org/10.1021/acs.jpcc.7b01314>.
- [41] N.K. Elumalai, A. Uddin, Open circuit voltage of organic solar cells: an in-depth review, *Energy Environ. Sci.* 9 (2016) 391–410, <https://doi.org/10.1039/C5EE02871J>.
- [42] V.A. Trukhanov, V.V. Bruevich, D.Y. Paraschuk, Fill factor in organic solar cells can exceed the Shockley–Queisser limit, *Sci. Rep.* 5 (2015), 11478, <https://doi.org/10.1038/srep11478>.
- [43] W. Li, K.H. Hendriks, W.S.C. Roelofs, Y. Kim, M.M. Wienk, R.A.J. Janssen, Efficient small bandgap polymer solar cells with high fill factors for 300 nm thick films, *Adv. Mater.* 25 (2013) 3182–3186, <https://doi.org/10.1002/adma.201300017>.
- [44] T.L. Nguyen, H. Choi, S.-J. Ko, M.A. Uddin, B. Walker, S. Yum, J.-E. Jeong, M. H. Yun, T.J. Shin, S. Hwang, J.Y. Kim, H.Y. Woo, Semi-crystalline photovoltaic polymers with efficiency exceeding 9% in a ~300 nm thick conventional single-cell device, *Energy Environ. Sci.* 7 (2014) 3040–3051, <https://doi.org/10.1039/C4EE01529K>.
- [45] Z. Fei, F.D. Eisner, X. Jiao, M. Azzouzi, J.A. Röhr, Y. Han, M. Shahid, A.S. R. Chesman, C.D. Easton, C.R. McNeill, T.D. Anthopoulos, J. Nelson, M. Heeney, An alkylated indaceno[3,2-b]thiophene-based nonfullerene acceptor with high crystallinity exhibiting single junction solar cell efficiencies greater than 13% with low voltage losses, *Adv. Mater.* 30 (2018), 1705209, <https://doi.org/10.1002/adma.201705209>.
- [46] Y. Cui, H. Yao, J. Zhang, K. Xian, T. Zhang, L. Hong, Y. Wang, Y. Xu, K. Ma, C. An, C. He, Z. Wei, F. Gao, J. Hou, Single-junction organic photovoltaic cells with approaching 18% efficiency, *Adv. Mater.* 32 (2020), 1908205, <https://doi.org/10.1002/adma.201908205>.
- [47] X. Guo, C. Cui, M. Zhang, L. Huo, Y. Huang, J. Hou, Y. Li, High efficiency polymer solar cells based on poly(3-hexylthiophene)/indene-C70 bisadduct with solvent additive, *Energy Environ. Sci.* 5 (2012) 7943–7949, <https://doi.org/10.1039/C2EE21481D>.
- [48] C. Hou, H. Yu, Modifying the nanostructures of PEDOT:PSS/Ti3C2TX composite hole transport layers for highly efficient polymer solar cells, *J. Mater. Chem. C* 8 (2020) 4169–4180, <https://doi.org/10.1039/D0TC00075B>.
- [49] J. Dong, J. Guo, X. Wang, P. Dong, Z. Wang, Y. Zhou, Y. Miao, B. Zhao, Y. Hao, H. Wang, B. Xu, S. Yin, A low-temperature solution-processed CuSCN/polymer hole transporting layer enables high efficiency for organic solar cells, *ACS Appl. Mater. Interfaces* 12 (2020) 46373–46380, <https://doi.org/10.1021/acsmami.0c12845>.
- [50] X. Li, X. Duan, Z. Liang, L. Yan, Y. Yang, J. Qiao, X. Hao, C. Zhang, J. Zhang, Y. Li, F. Huang, Y. Sun, Benzol[1,2-b:4,5-b']difuran based polymer donor for high-efficiency (>16%) and stable organic solar cells, *Adv. Energy Mater.* 12 (2022), 2103684, <https://doi.org/10.1002/aenm.202103684>.
- [51] S. Wen, Y. Li, T. Rath, Y. Li, Y. Wu, X. Bao, L. Han, H. Ehmann, G. Trimmel, Y. Zhang, R. Yang, A benzobis(thiazole)-based copolymer for highly efficient nonfullerene polymer solar cells, *Chem. Mater.* 31 (2019) 919–926, <https://doi.org/10.1021/acs.chemmater.8b04265>.
- [52] W. Zhao, S. Li, H. Yao, S. Zhang, Y. Zhang, B. Yang, J. Hou, Molecular optimization enables over 13% efficiency in organic solar cells, *J. Am. Chem. Soc.* 139 (2017) 7148–7151, <https://doi.org/10.1021/jacs.7b02677>.
- [53] S. Li, L. Ye, W. Zhao, S. Zhang, S. Mukherjee, H. Ade, J. Hou, Energy-level modulation of small-molecule electron acceptors to achieve over 12% efficiency in polymer solar cells, *Adv. Mater.* 28 (2016) 9423–9429, <https://doi.org/10.1002/adma.201602276>.
- [54] X. Song, N. Gasparini, L. Ye, H. Yao, J. Hou, H. Ade, D. Baran, Controlling blend morphology for ultrahigh current density in nonfullerene acceptor-based organic solar cells, *ACS Energy Lett.* 3 (2018) 669–676, <https://doi.org/10.1021/acsenergylett.7b01266>.
- [55] Y. Xie, H.S. Ryu, L. Han, Y. Cai, X. Duan, D. Wei, H.Y. Woo, Y. Sun, High-efficiency organic solar cells enabled by an alcohol-washable solid additive, *Sci. China Chem.* 64 (2021) 2161–2168, <https://doi.org/10.1007/s11426-021-1121-y>.
- [56] J. Wang, Y. Wang, P. Bi, Z. Chen, J. Qiao, J. Li, W. Wang, Z. Zheng, S. Zhang, X. Hao, J. Hou, Binary Organic Solar Cells with 19.2% Efficiency Enabled by Solid Additive, *Advanced Materials.* n/a (n.d.) 2301583. <https://doi.org/10.1002/adma.202301583>.
- [57] J. Yuan, Y. Zhang, L. Zhou, G. Zhang, H.-L. Yip, T.-K. Lau, X. Lu, C. Zhu, H. Peng, P.A. Johnson, M. Leclerc, Y. Cao, J. Ulanski, Y. Li, Y. Zou, Single-junction organic solar cell with over 15% efficiency using fused-ring acceptor with electron-deficient core, *Joule* 3 (2019) 1140–1151, <https://doi.org/10.1016/j.joule.2019.01.004>.
- [58] L. Yang, Z. Hu, Z. Zhang, J. Cao, H. Wang, J. Yu, F. Zhang, W. Tang, Molecular engineering of acceptors to control aggregation for optimized nonfullerene solar cells, *J. Mater. Chem. A* 8 (2020) 5458–5466, <https://doi.org/10.1039/DOTA00651C>.
- [59] M.B. Upama, N.K. Elumalai, M.A. Mahmud, C. Xu, D. Wang, M. Wright, A. Uddin, Enhanced electron transport enables over 12% efficiency by interface engineering of non-fullerene organic solar cells, *Sol. Energy Mater. Sol. Cell.* 187 (2018) 273–282, <https://doi.org/10.1016/j.solmat.2018.08.010>.
- [60] T. Duan, Q. Chen, Q. Yang, D. Hu, G. Cai, X. Lu, J. Lv, H. Song, C. Zhong, F. Liu, D. Yu, S. Lu, Simple thiazole-centered oligothiophene donor enables 15.4% efficiency all small molecule organic solar cells, *J. Mater. Chem. A* 10 (2022) 3009–3017, <https://doi.org/10.1039/D1TA09058E>.
- [61] X. Li, F. Pan, C. Sun, M. Zhang, Z. Wang, J. Du, J. Wang, M. Xiao, L. Xue, Z.-G. Zhang, C. Zhang, F. Liu, Y. Li, Simplified synthetic routes for low cost and high photovoltaic performance n-type organic semiconductor acceptors, *Nat. Commun.* 10 (2019) 519, <https://doi.org/10.1038/s41467-019-08508-3>.
- [62] P. Jiang, S. Ming, Q.-Q. Jia, Y. Liu, H. Lu, M. Li, X. Xu, H.-B. Li, Z. Bo, The influence of the π -bridging unit of fused-ring acceptors on the performance of organic solar cells, *J. Mater. Chem. A* 6 (2018) 21335–21340, <https://doi.org/10.1039/C8TA08410F>.
- [63] H. Chen, D. Hu, Q. Yang, J. Gao, J. Fu, K. Yang, H. He, S. Chen, Z. Kan, T. Duan, C. Yang, J. Ouyang, Z. Xiao, K. Sun, S. Lu, All-small-molecule organic solar cells with an ordered liquid crystalline donor, *Joule* 3 (2019) 3034–3047, <https://doi.org/10.1016/j.joule.2019.09.009>.
- [64] Q. Liu, Y. Jiang, K. Jin, J. Qin, J. Xu, W. Li, J. Xiong, J. Liu, Z. Xiao, K. Sun, S. Yang, X. Zhang, L. Ding, 18% Efficiency organic solar cells, *Sci. Bull.* 65 (2020) 272–275, <https://doi.org/10.1016/j.scib.2020.01.001>.
- [65] X. Ma, W. Xu, Z. Liu, S.Y. Jeong, C. Xu, J. Zhang, H.Y. Woo, Z. Zhou, F. Zhang, Over 18.1% efficiency of layer-by-layer polymer solar cells by enhancing exciton utilization near the ITO electrode, *ACS Appl. Mater. Interfaces* 15 (2023) 7247–7254, <https://doi.org/10.1021/acsami.2c22461>.
- [66] Y. Liang, Z. Xu, J. Xia, S.-T. Tsai, Y. Wu, G. Li, C. Ray, L. Yu, For the bright future—bulk heterojunction polymer solar cells with power conversion efficiency of 7.4, *Adv. Mater.* 22 (2010), <https://doi.org/10.1002/adma.200903528>.
- [67] S.H. Park, A. Roy, S. Beaupré, S. Cho, N. Coates, J.S. Moon, D. Moses, M. Leclerc, K. Lee, A.J. Heeger, Bulk heterojunction solar cells with internal quantum efficiency approaching 100, *Nat. Photonics* 3 (2009) 297–302, <https://doi.org/10.1038/nphoton.2009.69>.
- [68] S.-H. Liao, H.-J. Jhuo, Y.-S. Cheng, S.-A. Chen, Fullerene derivative-doped zinc oxide nanofilm as the cathode of inverted polymer solar cells with low-bandgap polymer (PTB7-TH) for high performance, *Adv. Mater.* 25 (2013) 4766–4771, <https://doi.org/10.1002/adma.201301476>.
- [69] Y. Liu, J. Zhao, Z. Li, C. Mu, W. Ma, H. Hu, K. Jiang, H. Lin, H. Ade, H. Yan, Aggregation and morphology control enables multiple cases of high-efficiency polymer solar cells, *Nat. Commun.* 5 (2014) 5293, <https://doi.org/10.1038/ncomms5293>.
- [70] C. Zhan, J. Yao, More than conformational “twisting” or “coplanarity”: molecular strategies for designing high-efficiency nonfullerene organic solar cells, *Chem. Mater.* 28 (2016) 1948–1964, <https://doi.org/10.1021/acs.chemmater.5b04339>.
- [71] C. Li, X. Zhang, N. Yu, X. Gu, L. Qin, Y. Wei, X. Liu, J. Zhang, Z. Wei, Z. Tang, Q. Shi, H. Huang, Simple nonfused-ring electron acceptors with noncovalently conformational locks for low-cost and high-performance organic solar cells

- enabled by end-group engineering, *Adv. Funct. Mater.* 32 (2022), 2108861, <https://doi.org/10.1002/adfm.202108861>.
- [72] X. Zhang, L. Qin, J. Yu, Y. Li, Y. Wei, X. Liu, X. Lu, F. Gao, H. Huang, High-performance noncovalently fused-ring electron acceptors for organic solar cells enabled by noncovalent intramolecular interactions and end-group engineering, *Angew. Chem. Int. Ed.* 60 (2021) 12475–12481, <https://doi.org/10.1002/anie.202100390>.
- [73] X. Zhang, C. Li, L. Qin, H. Chen, J. Yu, Y. Wei, X. Liu, J. Zhang, Z. Wei, F. Gao, Q. Peng, H. Huang, Side-chain engineering for enhancing the molecular rigidity and photovoltaic performance of noncovalently fused-ring electron acceptors, *Angew. Chem. Int. Ed.* 60 (2021) 17720–17725, <https://doi.org/10.1002/anie.202106753>.
- [74] T. Dong, L. Lv, L. Feng, Y. Xia, W. Deng, P. Ye, B. Yang, S. Ding, A. Facchetti, H. Dong, H. Huang, Noncovalent Se···O conformational locks for constructing high-performing optoelectronic conjugated polymers, *Adv. Mater.* 29 (2017), 1606025, <https://doi.org/10.1002/adma.201606025>.
- [75] N. Gasparini, X. Jiao, T. Heumueller, D. Baran, G.J. Matt, S. Pladischer, E. Spiecker, H. Ade, C.J. Brabec, T. Ameri, Designing ternary blend bulk heterojunction solar cells with reduced carrier recombination and a fill factor of 77, *Nat. Energy* 1 (2016), 16118, <https://doi.org/10.1038/nenergy.2016.118>.
- [76] J. Gao, X. Ma, C. Xu, X. Wang, J.H. Son, S.Y. Jeong, Y. Zhang, C. Zhang, K. Wang, L. Niu, J. Zhang, H.Y. Woo, J. Zhang, F. Zhang, Over 17.7% efficiency ternary-blend organic solar cells with low energy-loss and good thickness-tolerance, *Chem. Eng. J.* 428 (2022), 129276, <https://doi.org/10.1016/j.cej.2021.129276>.
- [77] N.Y. Doumon, L. Yang, F. Rosei, Ternary organic solar cells: a review of the role of the third element, *Nano Energy* 94 (2022), 106915, <https://doi.org/10.1016/j.nanoen.2021.106915>.
- [78] X. Du, J. Zhao, H. Zhang, X. Lu, L. Zhou, Z. Chen, H. Lin, C. Zheng, S. Tao, Modulating the molecular packing and distribution enables fullerene-free ternary organic solar cells with high efficiency and long shelf-life, *J. Mater. Chem. A* 7 (2019) 20139–20150, <https://doi.org/10.1039/C9TA07542A>.
- [79] L. Chang, M. Sheng, L. Duan, A. Uddin, Ternary organic solar cells based on nonfullerene acceptors: a review, *Org. Electron.* 90 (2021), 106063, <https://doi.org/10.1016/j.orgel.2021.106063>.
- [80] T. Yan, J. Ge, T. Lei, W. Zhang, W. Song, B. Fanady, D. Zhang, S. Chen, R. Peng, Z. Ge, 16.55% efficiency ternary organic solar cells enabled by incorporating a small molecular donor, *J. Mater. Chem. A* 7 (2019) 25894–25899, <https://doi.org/10.1039/C9TA0145D>.
- [81] K. Yu, W. Song, Y. Li, Z. Chen, J. Ge, D. Yang, J. Zhang, L. Xie, C. Liu, Z. Ge, Achieving 18.14% efficiency of ternary organic solar cells with alloyed nonfullerene acceptor, *Small Structures* 2 (2021), 2100099, <https://doi.org/10.1002/sstr.202100099>.
- [82] S. Dai, S. Chandrabose, J. Xin, T. Li, K. Chen, P. Xue, K. Liu, K. Zhou, W. Ma, J. M. Hodgkiss, X. Zhan, High-performance organic solar cells based on polymer donor/small molecule donor/nonfullerene acceptor ternary blends, *J. Mater. Chem. A* 7 (2019) 2268–2274, <https://doi.org/10.1039/C8TA11637G>.
- [83] D. Li, L. Zhu, X. Liu, W. Xiao, J. Yang, R. Ma, L. Ding, F. Liu, C. Duan, M. Fahlman, Q. Bao, Enhanced and balanced charge transport boosting ternary solar cells over 17% efficiency, *Adv. Mater.* 32 (2020), e2002344, <https://doi.org/10.1002/adma.202002344>.
- [84] Q. An, J. Wang, X. Ma, J. Gao, Z. Hu, B. Liu, H. Sun, X. Guo, X. Zhang, F. Zhang, Two compatible polymer donors contribute synergistically for ternary organic solar cells with 17.53% efficiency, *Energy Environ. Sci.* 13 (2020) 5039–5047, <https://doi.org/10.1039/D0EE02516J>.
- [85] T. Zhang, C. An, P. Bi, Q. Lv, J. Qin, L. Hong, Y. Cui, S. Zhang, J. Hou, A thiadiazole-based conjugated polymer with ultradeep HOMO level and strong electroluminescence enables 18.6% efficiency in organic solar cell, *Adv. Energy Mater.* 11 (2021), 2101705, <https://doi.org/10.1002/aenm.202101705>.
- [86] L. Zhang, X. Xu, B. Lin, H. Zhao, T. Li, J. Xin, Z. Bi, G. Qiu, S. Guo, K. Zhou, X. Zhan, W. Ma, Achieving balanced crystallinity of donor and acceptor by combining blade-coating and ternary strategies in organic solar cells, *Adv. Mater.* 30 (2018), 1805041, <https://doi.org/10.1002/adma.201805041>.
- [87] L. Zhang, S. Li, T.-K. Lau, Y. Cui, X. Lu, M. Shi, C.-Z. Li, H. Li, J. Hou, H. Chen, Over 17% efficiency ternary organic solar cells enabled by two non-fullerene acceptors working in an alloy-like model, *Energy Environ. Sci.* 13 (2020) 635–645, <https://doi.org/10.1039/C9EE03710A>.
- [88] X. Ma, A. Zeng, J. Gao, Z. Hu, C. Xu, J.H. Son, S.Y. Jeong, C. Zhang, M. Li, K. Wang, H. Yan, Z. Ma, Y. Wang, H.Y. Woo, F. Zhang, Approaching 18% efficiency of ternary organic photovoltaics with wide bandgap polymer donor and well compatible Y6 : Y6-1O as acceptor, *Natl. Sci. Rev.* 8 (2021), <https://doi.org/10.1093/nsr/nwaa305>.
- [89] J.D. Servaites, M.A. Ratner, T.J. Marks, Organic solar cells: a new look at traditional models, *Energy Environ. Sci.* 4 (2011) 4410–4422, <https://doi.org/10.1039/C1EE01663F>.
- [90] C. Yi, X. Hu, X. Gong, A. Elzatahry, Interfacial engineering for high performance organic photovoltaics, *Mater. Today* 19 (2016) 169–177, <https://doi.org/10.1016/j.mattod.2015.10.003>.
- [91] Y. He, Y. Li, Fullerene derivative acceptors for high performance polymer solar cells, *Phys. Chem. Chem. Phys.* 13 (2011) 1970–1983, <https://doi.org/10.1039/C0CP01178A>.
- [92] H. Tan, Y. Long, J. Zhang, J. Zhu, J. Yang, J. Yu, W. Zhu, Spirobifluorene-cored wide bandgap non-fullerene small molecular acceptor with 3D structure for organic solar cells, *Dyes Pigments* 162 (2019) 797–801, <https://doi.org/10.1016/j.dyepig.2018.11.016>.
- [93] C. Yan, S. Barlow, Z. Wang, H. Yan, A.K.-Y. Jen, S.R. Marder, X. Zhan, Nonfullerene acceptors for organic solar cells, *Nat. Rev. Mater.* 3 (2018), 18003, <https://doi.org/10.1038/natrevmats.2018.3>.
- [94] Y. Cui, H. Yao, J. Zhang, T. Zhang, Y. Wang, L. Hong, K. Xian, B. Xu, S. Zhang, J. Peng, Z. Wei, F. Gao, J. Hou, Over 16% efficiency organic photovoltaic cells enabled by a chlorinated acceptor with increased open-circuit voltages, *Nat. Commun.* 10 (2019) 2515, <https://doi.org/10.1038/s41467-019-10351-5>.
- [95] G. Chai, Y. Chang, J. Zhang, X. Xu, L. Yu, X. Zou, X. Li, Y. Chen, S. Luo, B. Liu, F. Bai, Z. Luo, H. Yu, J. Liang, T. Liu, K.S. Wong, H. Zhou, Q. Peng, H. Yan, Fine-tuning of side-chain orientations on nonfullerene acceptors enables organic solar cells with 17.7% efficiency, *Energy Environ. Sci.* 14 (2021) 3469–3479, <https://doi.org/10.1039/D0EE03506H>.
- [96] X. Xu, T. Yu, Z. Bi, W. Ma, Y. Li, Q. Peng, Realizing over 13% efficiency in green-solvent-processed nonfullerene organic solar cells enabled by 1,3,4-thiadiazole-based wide-bandgap copolymers, *Adv. Mater.* 30 (2018), 1703973, <https://doi.org/10.1002/adma.201703973>.
- [97] H. Yao, Y. Cui, D. Qian, C.S. Ponseca, A. Honarfar, Y. Xu, J. Xin, Z. Chen, L. Hong, B. Gao, R. Yu, Y. Zu, W. Ma, P. Chabera, T. Pullerits, A. Yartsev, F. Gao, J. Hou, 14.7% efficiency organic photovoltaic cells enabled by active materials with a large electrostatic potential difference, *J. Am. Chem. Soc.* 141 (2019) 7743–7750, <https://doi.org/10.1021/jacs.8b12937>.
- [98] S. Feng, C. Zhang, Z. Bi, Y. Liu, P. Jiang, S. Ming, X. Xu, W. Ma, Z. Bo, Controlling molecular packing and orientation via constructing a ladder-type electron acceptor with asymmetric substituents for thick-film nonfullerene solar cells, *ACS Appl. Mater. Interfaces* 10 (2018), <https://doi.org/10.1021/acsami.8b19596>. (Accessed 11 October 2022).
- [99] J. Yuan, T. Huang, P. Cheng, Y. Zou, H. Zhang, J.L. Yang, S.-Y. Chang, Z. Zhang, W. Huang, R. Wang, D. Meng, F. Gao, Y. Yang, Enabling low voltage losses and high photocurrent in fullerene-free organic photovoltaics, *Nat. Commun.* 10 (2019) 570, <https://doi.org/10.1038/s41467-019-08386-9>.
- [100] H. Kang, G. Kim, J. Kim, S. Kwon, H. Kim, K. Lee, Bulk-heterojunction organic solar cells: five core technologies for their commercialization, *Adv. Mater.* 28 (2016) 7821–7861, <https://doi.org/10.1002/adma.201601197>.
- [101] F. Liu, C. Xiao, G. Feng, C. Li, Y. Wu, E. Zhou, W. Li, End group engineering on the side chains of conjugated polymers toward efficient non-fullerene organic solar cells, *ACS Appl. Mater. Interfaces* 12 (2020) 6151–6158, <https://doi.org/10.1021/acsami.9b22275>.
- [102] Y. Cai, L. Huo, Y. Sun, Recent advances in wide-bandgap photovoltaic polymers, *Adv. Mater.* 29 (2017), 1605437, <https://doi.org/10.1002/adma.201605437>.
- [103] G. Li, V. Shrotriya, J. Huang, Y. Yao, T. Moriarty, K. Emery, Y. Yang, High-efficiency solution processable polymer photovoltaic cells by self-organization of polymer blends, *Nat. Mater.* 4 (2005) 864–868, <https://doi.org/10.1038/nmat1500>.
- [104] M.M. Wienk, J.M. Kroon, W.J.H. Verhees, J. Knol, J.C. Hummelen, P.A. van Hal, R.A.J. Janssen, Efficient methano[70]fullerene/MDMO-PPV bulk heterojunction photovoltaic cells, *Angew. Chem. Int. Ed.* 42 (2003) 3371–3375, <https://doi.org/10.1002/anie.200351647>.
- [105] P. Schilinsky, C. Waldauf, C.J. Brabec, Recombination and loss analysis in polythiophene based bulk heterojunction photodetectors, *Appl. Phys. Lett.* 81 (2002) 3885–3887, <https://doi.org/10.1063/1.1521244>.
- [106] T. Erb, U. Zhokhavets, G. Gobsch, S. Raleva, B. Stühn, P. Schilinsky, C. Waldauf, C.J. Brabec, Correlation between structural and optical properties of composite polymer/fullerene films for organic solar cells, *Adv. Funct. Mater.* 15 (2005) 1193–1196, <https://doi.org/10.1002/adfm.200400521>.
- [107] H.-Y. Chen, J. Hou, S. Zhang, Y. Liang, G. Yang, Y. Yang, L. Yu, Y. Wu, G. Li, Polymer solar cells with enhanced open-circuit voltage and efficiency, *Nat. Photonics* 3 (2009) 649–653, <https://doi.org/10.1038/nphoton.2009.192>.
- [108] J.-D. Chen, C. Cui, Y.-Q. Li, L. Zhou, Q.-D. Ou, C. Li, Y. Li, J.-X. Tang, Single-junction polymer solar cells exceeding 10% power conversion efficiency, *Adv. Mater.* 27 (2015) 1035–1041, <https://doi.org/10.1002/adma.201404535>.
- [109] W. Zhao, D. Qian, S. Zhang, S. Li, O. Inganäs, F. Gao, J. Hou, Fullerene-free polymer solar cells with over 11% efficiency and excellent thermal stability, *Adv. Mater.* 28 (2016) 4734–4739, <https://doi.org/10.1002/adma.201600281>.
- [110] W. Xu, M. Zhang, J. Xiao, M. Zeng, L. Ye, C. Weng, B. Zhao, J. Zhang, S. Tan, Improved photovoltaic properties of PM6-based terpolymer donors containing benzothiadiazole with a siloxane-terminated side chain, *Polym. Chem.* 11 (2020) 6178–6186, <https://doi.org/10.1039/DOPY00890G>.
- [111] L. Wang, C. Guo, X. Zhang, S. Cheng, D. Li, J. Cai, C. Chen, Y. Fu, J. Zhou, H. Qin, D. Liu, T. Wang, Alkyl chain tuning of non-fullerene electron acceptors toward 18.2% efficiency binary organic solar cells, *Chem. Mater.* 33 (2021) 8854–8862, <https://doi.org/10.1021/acs.chemmater.1c03104>.
- [112] B. Qiu, Z. Chen, S. Qin, J. Yao, W. Huang, L. Meng, H. Zhu, Y. Michael, Yang, Z.-G. Zhang, Y. Li, Highly efficient all-small-molecule organic solar cells with appropriate active layer morphology by side chain engineering of donor molecules and thermal annealing, *Adv. Mater.* 32 (2020), 1908373, <https://doi.org/10.1002/adma.201908373>.
- [113] R. Zhou, C. Yang, W. Zou, M. Abdullah Adil, H. Li, M. Lv, Z. Huang, M. Lv, J. Zhang, K. Lu, Z. Wei, Combining chlorination and sulfuration strategies for high-performance all-small-molecule organic solar cells, *J. Energy Chem.* 52 (2021) 228–233, <https://doi.org/10.1016/j.jechem.2020.04.041>.
- [114] T. Duan, J. Gao, T. Xu, Z. Kan, W. Chen, R. Singh, G.P. Kini, C. Zhong, D. Yu, Z. Xiao, Z. Xiao, S. Lu, Simple organic donors based on halogenated oligothiophenes for all small molecule solar cells with efficiency over 11, *J. Mater. Chem. A* 8 (2020) 5843–5847, <https://doi.org/10.1039/DOTA00159G>.
- [115] X. Chen, Q. Zhang, D. Wang, X. Xu, Z. Wang, Y. Li, H. Zhu, X. Lu, W. Chen, H. Qiu, C.-Z. Li, High-efficiency ternary organic solar cells based on the synergized

- polymeric and small-molecule donors, *Solar RRL* 4 (2020), 2000537, <https://doi.org/10.1002/solr.202000537>.
- [116] Q. An, J. Wang, F. Zhang, Ternary polymer solar cells with alloyed donor achieving 14.13% efficiency and 78.4% fill factor, *Nano Energy* 60 (2019) 768–774, <https://doi.org/10.1016/j.nanoen.2019.04.018>.
- [117] J. Song, C. Li, L. Zhu, J. Guo, J. Xu, X. Zhang, K. Weng, K. Zhang, J. Min, X. Hao, Y. Zhang, F. Liu, Y. Sun, Ternary organic solar cells with efficiency >16.5% based on two compatible nonfullerene acceptors, *Adv. Mater.* 31 (2019), 1905645, <https://doi.org/10.1002/adma.201905645>.
- [118] P. Bi, S. Zhang, Z. Chen, Y. Xu, Y. Cui, T. Zhang, J. Ren, J. Qin, L. Hong, X. Hao, J. Hou, Reduced non-radiative charge recombination enables organic photovoltaic cell approaching 19% efficiency, *Joule* 5 (2021) 2408–2419, <https://doi.org/10.1016/j.joule.2021.06.020>.
- [119] L. Zhan, S. Li, X. Xia, Y. Li, X. Lu, L. Zuo, M. Shi, H. Chen, Layer-by-Layer processed ternary organic photovoltaics with efficiency over 18%, *Adv. Mater.* 33 (2021), 2007231, <https://doi.org/10.1002/adma.202007231>.
- [120] T. Liu, R. Ma, Z. Luo, Y. Guo, G. Zhang, Y. Xiao, T. Yang, Y. Chen, G. Li, Y. Yi, X. Lu, H. Yan, B. Tang, Concurrent improvement in JSC and VOC in high-efficiency ternary organic solar cells enabled by a red-absorbing small-molecule acceptor with a high LUMO level, *Energy Environ. Sci.* 13 (2020) 2115–2123, <https://doi.org/10.1039/D0EE00662A>.
- [121] K. Li, Y. Wu, Y. Tang, M.-A. Pan, W. Ma, H. Fu, C. Zhan, J. Yao, Ternary blended fullerene-free polymer solar cells with 16.5% efficiency enabled with a higher-LUMO-level acceptor to improve film morphology, *Adv. Energy Mater.* 9 (2019), 1901728, <https://doi.org/10.1002/aenm.201901728>.
- [122] S. Liu, D. Chen, X. Hu, Z. Xing, J. Wan, L. Zhang, L. Tan, W. Zhou, Y. Chen, Printable and large-area organic solar cells enabled by a ternary pseudo-planar heterojunction strategy, *Adv. Funct. Mater.* 30 (2020), 2003223, <https://doi.org/10.1002/adfm.202003223>.
- [123] S. Zhang, X. Ma, L. Niu, S.Y. Jeong, H.Y. Woo, Z. Zhou, F. Zhang, 18.66% efficiency of polymer solar cells employing two nonfullerene acceptors with fluorine or chlorine substitution, *Solar RRL* 7 (2023), 2200957, <https://doi.org/10.1002/solr.202200957>.
- [124] M. Jiang, H.-F. Zhi, B. Zhang, C. Yang, A. Mahmood, M. Zhang, H.Y. Woo, F. Zhang, J.-L. Wang, Q. An, controlling morphology and voltage loss with ternary strategy triggers efficient all-small-molecule organic solar cells, *ACS Energy Lett.* 8 (2023) 1058–1067, <https://doi.org/10.1021/acsenergylett.2c02348>.
- [125] L. Zhu, M. Zhang, J. Xu, C. Li, J. Yan, G. Zhou, W. Zhong, T. Hao, J. Song, X. Xue, Z. Zhou, R. Zeng, H. Zhu, C.-C. Chen, R.C.I. MacKenzie, Y. Zou, J. Nelson, Y. Zhang, Y. Sun, F. Liu, Single-junction organic solar cells with over 19% efficiency enabled by a refined double-fibril network morphology, *Nat. Mater.* 21 (2022) 656–663, <https://doi.org/10.1038/s41563-022-01244-y>.
- [126] J. Gao, N. Yu, Z. Chen, Y. Wei, C. Li, T. Liu, X. Gu, J. Zhang, Z. Wei, Z. Tang, X. Hao, F. Zhang, X. Zhang, H. Huang, Over 19.2% efficiency of organic solar cells enabled by precisely tuning the charge transfer state via donor alloy strategy, *Adv. Sci.* 9 (2022), 2203606, <https://doi.org/10.1002/advs.202203606>.
- [127] T. Ameri, G. Dennler, C. Lungenschmid, C.J. Brabec, Organic tandem solar cells: a review, *Energy Environ. Sci.* 2 (2009) 347–363, <https://doi.org/10.1039/B817952B>.
- [128] A.D. Vos, Detailed balance limit of the efficiency of tandem solar cells, *J. Phys. D Appl. Phys.* 13 (1980) 839, <https://doi.org/10.1088/0022-3727/13/5/018>.
- [129] P. Cheng, G. Li, X. Zhan, Y. Yang, Next-generation organic photovoltaics based on non-fullerene acceptors, *Nat. Photonics* 12 (2018) 131–142, <https://doi.org/10.1038/s41566-018-0104-9>.
- [130] T. Ameri, N. Li, C.J. Brabec, Highly efficient organic tandem solar cells: a follow up review, *Energy Environ. Sci.* 6 (2013) 2390–2413, <https://doi.org/10.1039/C3EE40388B>.
- [131] Y. Cui, H. Yao, B. Gao, Y. Qin, S. Zhang, B. Yang, C. He, B. Xu, J. Hou, Fine-tuned photoactive and interconnection layers for achieving over 13% efficiency in a fullerene-free tandem organic solar cell, *J. Am. Chem. Soc.* 139 (2017) 7302–7309, <https://doi.org/10.1021/jacs.7b01493>.
- [132] M. Li, K. Gao, X. Wan, Q. Zhang, B. Kan, R. Xia, F. Liu, X. Yang, H. Feng, W. Ni, Y. Wang, J. Peng, H. Zhang, Z. Liang, H.-L. Yip, X. Peng, Y. Cao, Y. Chen, Solution-processed organic tandem solar cells with power conversion efficiencies >12%, *Nat. Photonics* 11 (2017) 85–90, <https://doi.org/10.1038/nphoton.2016.240>.
- [133] Z. Shi, Y. Bai, X. Chen, R. Zeng, Z. Tan, Tandem structure: a breakthrough in power conversion efficiency for highly efficient polymer solar cells, *Sustain. Energy Fuels* 3 (2019) 910–934, <https://doi.org/10.1039/C8SE00601F>.
- [134] Y. Qin, Y. Chen, Y. Cui, S. Zhang, H. Yao, J. Huang, W. Li, Z. Zheng, J. Hou, Achieving 12.8% efficiency by simultaneously improving open-circuit voltage and short-circuit current density in tandem organic solar cells, *Adv. Mater.* 29 (2017), 1606340, <https://doi.org/10.1002/adma.201606340>.
- [135] C.H.Y. Ho, T. Kim, Y. Xiong, Y. Firdaus, X. Yi, Q. Dong, J.J. Rech, A. Gadisa, R. Booth, B.T. O'Connor, A. Amassian, H. Ade, W. You, T.D. Anthopoulos, F. So, High-performance tandem organic solar cells using HSolar as the interconnecting layer, *Adv. Energy Mater.* 10 (2020), 2000823, <https://doi.org/10.1002/aenm.202000823>.
- [136] G. Liu, J. Jia, K. Zhang, X. Jia, Q. Yin, W. Zhong, L. Li, F. Huang, Y. Cao, 15% efficiency tandem organic solar cell based on a novel highly efficient wide-bandgap nonfullerene acceptor with low energy loss, *Adv. Energy Mater.* 9 (2019), 1803657, <https://doi.org/10.1002/aenm.201803657>.
- [137] S. Zhang, Y. Qin, M.A. Uddin, B. Jang, W. Zhao, D. Liu, H.Y. Woo, J. Hou, A fluorinated polythiophene derivative with stabilized backbone conformation for highly efficient fullerene and non-fullerene polymer solar cells, *Macromolecules* 49 (2016) 2993–3000, <https://doi.org/10.1021/acs.macromol.6b00248>.
- [138] G. Liu, R. Xia, Q. Huang, K. Zhang, Z. Hu, T. Jia, X. Liu, H.-L. Yip, F. Huang, Tandem organic solar cells with 18.7% efficiency enabled by suppressing the charge recombination in front sub-cell, *Adv. Funct. Mater.* 31 (2021), 2103283, <https://doi.org/10.1002/adfm.202103283>.
- [139] X. Che, Y. Li, Y. Qu, S.R. Forrest, High fabrication yield organic tandem photovoltaics combining vacuum- and solution-processed subcells with 15% efficiency, *Nat. Energy* 3 (2018) 422–427, <https://doi.org/10.1038/s41560-018-0134-z>.
- [140] S. Qin, Z. Jia, L. Meng, C. Zhu, W. Lai, J. Zhang, W. Huang, C. Sun, B. Qiu, Y. Li, Non-halogenated-solvent processed and additive-free tandem organic solar cell with efficiency reaching 16.67, *Adv. Funct. Mater.* 31 (2021), 2102361, <https://doi.org/10.1002/adfm.202102361>.
- [141] Z. Zheng, J. Wang, P. Bi, J. Ren, Y. Wang, Y. Yang, X. Liu, S. Zhang, J. Hou, Tandem organic solar cell with 20.2% efficiency, *Joule* 6 (2022) 171–184, <https://doi.org/10.1016/j.joule.2021.12.017>.
- [142] Y. Liu, C.-C. Chen, Z. Hong, J. Gao, Y. Michael Yang, H. Zhou, L. Dou, G. Li, Y. Yang, Solution-processed small-molecule solar cells: breaking the 10% power conversion efficiency, *Sci. Rep.* 3 (2013) 3356, <https://doi.org/10.1038/srep03356>.
- [143] J. Wang, Z. Zheng, P. Bi, Z. Chen, Y. Wang, X. Liu, S. Zhang, X. Hao, M. Zhang, Y. Li, J. Hou, Tandem organic solar cells with 20.6% efficiency enabled by reduced voltage losses, *Natl. Sci. Rev.* (2023) nwad085, <https://doi.org/10.1093/nsr/nwad085>.
- [144] Z. Jia, Q. Ma, Z. Chen, L. Meng, N. Jain, I. Angunawela, S. Qin, X. Kong, X. Li, Y. Michael Yang, H. Zhu, H. Ade, F. Gao, Y. Li, Near-infrared absorbing acceptor with suppressed triplet exciton generation enabling high performance tandem organic solar cells, *Nat. Commun.* 14 (2023) 1236, <https://doi.org/10.1038/s41467-023-36917-y>.
- [145] K. Yoshikawa, W. Yoshida, T. Irie, H. Kawasaki, K. Konishi, H. Ishibashi, T. Asatani, D. Adachi, M. Kanematsu, H. Uzu, K. Yamamoto, Exceeding conversion efficiency of 26% by heterojunction interdigitated back contact solar cell with thin film Si technology, *Sol. Energy Mater. Sol. Cell.* 173 (2017) 37–42, <https://doi.org/10.1016/j.solmat.2017.06.024>.
- [146] Risen Solar Panels: Now with 25-year Product Warranty, Solar Run, 2022, <http://www.solarrun.com.au/risen-solar-panels-now-with-25-year-product-warnty/>. (Accessed 26 October 2022).
- [147] X. Du, T. Heumueller, W. Gruber, A. Classen, T. Unruh, N. Li, C.J. Brabec, Efficient polymer solar cells based on non-fullerene acceptors with potential device lifetime approaching 10 years, *Joule* 3 (2019) 215–226, <https://doi.org/10.1016/j.joule.2018.09.001>.
- [148] Y. Zhang, I.D.W. Samuel, T. Wang, D.G. Lidzey, Current status of outdoor lifetime testing of organic photovoltaics, *Adv. Sci.* 5 (2018), 1800434, <https://doi.org/10.1002/advs.201800434>.
- [149] F. Zhao, C. Wang, X. Zhan, Morphology control in organic solar cells, *Adv. Energy Mater.* 8 (2018), 1703147, <https://doi.org/10.1002/aenm.201703147>.
- [150] H. Lee, C. Park, D.H. Sin, J.H. Park, K. Cho, Recent advances in morphology optimization for organic photovoltaics, *Adv. Mater.* 30 (2018), 1800453, <https://doi.org/10.1002/adma.201800453>.
- [151] R. Roesch, K.-R. Eberhardt, S. Engmann, G. Gobsch, H. Hoppe, Polymer solar cells with enhanced lifetime by improved electrode stability and sealing, *Sol. Energy Mater. Sol. Cell.* 117 (2013) 59–66, <https://doi.org/10.1016/j.solmat.2013.05.013>.
- [152] C.H. Peters, I.T. Sachs-Quintana, J.P. Kastrop, S. Beaupré, M. Leclerc, M. D. McGehee, High efficiency polymer solar cells with long operating lifetimes, *Adv. Energy Mater.* 1 (2011) 491–494, <https://doi.org/10.1002/aenm.201100138>.
- [153] C.H. Peters, I.T. Sachs-Quintana, W.R. Mateker, T. Heumueller, J. Rivnay, R. Noriega, Z.M. Bailey, E.T. Hoke, A. Salleo, M.D. McGehee, The mechanism of burn-in loss in a high efficiency polymer solar cell, *Adv. Mater.* 24 (2012) 663–668, <https://doi.org/10.1002/adma.201103010>.
- [154] R. Roesch, K.-R. Eberhardt, S. Engmann, G. Gobsch, H. Hoppe, Polymer solar cells with enhanced lifetime by improved electrode stability and sealing, *Sol. Energy Mater. Sol. Cell.* 117 (2013) 59–66, <https://doi.org/10.1016/j.solmat.2013.05.013>.
- [155] E.S.R. Bovill, J. Griffin, T. Wang, J.W. Kingsley, H. Yi, A. Iraqi, A.R. Buckley, D. G. Lidzey, Air processed organic photovoltaic devices incorporating a MoO_x anode buffer layer, *Appl. Phys. Lett.* 102 (2013), 183303, <https://doi.org/10.1063/1.4804294>.
- [156] A.J. Pearson, P.E. Hopkinson, E. Couderc, K. Domanski, M. Abdi-Jalebi, N. C. Greenham, Critical light instability in CB/DIO processed PBDTTT-EFT:PC71BM organic photovoltaic devices, *Org. Electron.* 30 (2016) 225–236, <https://doi.org/10.1016/j.orgel.2015.12.024>.
- [157] M. Ghasemi, N. Balar, Z. Peng, H. Hu, Y. Qin, T. Kim, J.J. Rech, M. Bidwell, W. Mask, I. McCulloch, W. You, A. Amassian, C. Risko, B.T. O'Connor, H. Ade, A molecular interaction-diffusion framework for predicting organic solar cell stability, *Nat. Mater.* 20 (2021) 525–532, <https://doi.org/10.1038/s41563-020-00872-6>.
- [158] Y. Qin, N. Balar, Z. Peng, A. Gadisa, I. Angunawela, A. Bagui, S. Kashani, J. Hou, H. Ade, The performance-stability conundrum of BTP-based organic solar cells, *Joule* 5 (2021) 2129–2147, <https://doi.org/10.1016/j.joule.2021.06.006>.
- [159] N.K. Zawacka, T.R. Andersen, J.W. Andreasen, L.H. Rossander, H.F. Dam, M. Jørgensen, F.C. Krebs, The influence of additives on the morphology and stability of roll-to-roll processed polymer solar cells studied through ex situ and in situ X-ray scattering, *J. Mater. Chem. A* 2 (2014) 18644–18654, <https://doi.org/10.1039/C4TA03484H>.

- [160] A. Tournebize, A. Rivaton, H. Peisert, T. Chassé, The crucial role of confined residual additives on the photostability of P3HT:PCBM active layers, *J. Phys. Chem. C* 119 (2015) 9142–9148, <https://doi.org/10.1021/acs.jpcc.5b01733>.
- [161] X. Wang, H.-J. Egelhaaf, H.-G. Mack, H. Azimi, C.J. Brabec, A.J. Meixner, D. Zhang, Morphology related photodegradation of low-band-gap polymer blends, *Adv. Energy Mater.* 4 (2014), 1400497, <https://doi.org/10.1002/aenm.201400497>.
- [162] W. Kim, J.K. Kim, E. Kim, T.K. Ahn, D.H. Wang, J.H. Park, Conflicted effects of a solvent additive on PTB7:PC71BM bulk heterojunction solar cells, *J. Phys. Chem. C* 119 (2015) 5954–5961, <https://doi.org/10.1021/jp510996w>.
- [163] W.R. Mateker, I.T. Sachs-Quintana, G.F. Burkhard, R. Cheacharoen, M. D. McGehee, Minimal long-term intrinsic degradation observed in a polymer solar cell illuminated in an oxygen-free environment, *Chem. Mater.* 27 (2015) 404–407, <https://doi.org/10.1021/cm504650a>.
- [164] S. Bishnoi, R. Datt, S. Arya, S. Gupta, R. Gupta, W.C. Tsai, S.N. Sharma, S. P. Patole, V. Gupta, Engineered cathode buffer layers for highly efficient organic solar cells: a review, *Adv. Mater. Interfac.* 9 (2022), 2101693, <https://doi.org/10.1002/admi.202101693>.
- [165] S.-Y. Park, H.-R. Kim, Y.-J. Kang, D.-H. Kim, J.-W. Kang, Organic solar cells employing magnetron sputtered p-type nickel oxide thin film as the anode buffer layer, *Sol. Energy Mater. Sol. Cell.* 94 (2010) 2332–2336, <https://doi.org/10.1016/j.solmat.2010.08.004>.
- [166] Y. Meng, Z. Hu, N. Ai, Z. Jiang, J. Wang, J. Peng, Y. Cao, Improving the stability of bulk heterojunction solar cells by incorporating pH-neutral PEDOT:PSS as the hole transport layer, *ACS Appl. Mater. Interfaces* 6 (2014) 5122–5129, <https://doi.org/10.1021/am500336s>.
- [167] A. Sharma, G. Andersson, D.A. Lewis, Role of humidity on indium and tin migration in organic photovoltaic devices, *Phys. Chem. Chem. Phys.* 13 (2011) 4381–4387, <https://doi.org/10.1039/C0CP02203A>.
- [168] S. Park, H.J. Son, Intrinsic photo-degradation and mechanism of polymer solar cells: the crucial role of non-fullerene acceptors, *J. Mater. Chem. A* 7 (2019) 25830–25837, <https://doi.org/10.1039/C9TA07417A>.
- [169] Y. Suh, S. Park, T. Lee, W. Chung, K. Kim, M. Kim, TEM study of stability of inverted photovoltaic (PV) cells, *Microsc. Microanal.* 16 (2010) 1378–1379, <https://doi.org/10.1017/S1431927610062057>.
- [170] S. Rafique, S.M. Abdullah, K. Sulaiman, M. Iwamoto, Layer by layer characterisation of the degradation process in PCDTBT:PC71BM based normal architecture polymer solar cells, *Org. Electron.* 40 (2017) 65–74, <https://doi.org/10.1016/j.orgel.2016.10.029>.
- [171] E. Voroshazi, G. Uytterhoeven, K. Cnops, T. Conard, P. Favia, H. Bender, R. Muller, D. Cheyns, Root-cause failure analysis of photocurrent loss in polythiophene:fullerene-based inverted solar cells, *ACS Appl. Mater. Interfaces* 7 (2015) 618–623, <https://doi.org/10.1021/am506771e>.
- [172] A.V. Hamza, J. Dykes, W.D. Mosley, L. Dinh, M. Balooch, Reaction and passivation of aluminum with C60, *Surf. Sci. Spec.* 318 (1994) 368–378, [https://doi.org/10.1016/0039-6028\(94\)90111-2](https://doi.org/10.1016/0039-6028(94)90111-2).
- [173] H. Habuchi, S. Nitta, D. Han, S. Nonomura, Localized electronic states related to O₂ intercalation and photoirradiation on C60 films and C70 films, *J. Appl. Phys.* 87 (2000) 8580–8588, <https://doi.org/10.1063/1.373582>.
- [174] H. Ishii, K. Seki, Energy level alignment at organic/metal interfaces studied by UV photoemission: breakdown of traditional assumption of a common vacuum level at the interface, *IEEE Trans. Electron. Dev.* 44 (1997) 1295–1301, <https://doi.org/10.1109/16.605471>.
- [175] A. Seemann, H.-J. Egelhaaf, C.J. Brabec, J.A. Hauch, Influence of oxygen on semi-transparent organic solar cells with gas permeable electrodes, *Org. Electron.* 10 (2009) 1424–1428, <https://doi.org/10.1016/j.orgel.2009.08.001>.
- [176] K. Norrman, M.V. Madsen, S.A. Gevorgyan, F.C. Krebs, Degradation patterns in water and oxygen of an inverted polymer solar cell, *J. Am. Chem. Soc.* 132 (2010) 16883–16892, <https://doi.org/10.1021/ja106299g>.
- [177] M. Lira-Cantu, K. Norrman, J.W. Andreasen, N. Casan-Pastor, F.C. Krebs, Detrimental effect of inert atmospheres on hybrid solar cells based on semiconductor oxides, *J. Electrochem. Soc.* 154 (2007) B508, <https://doi.org/10.1149/1.2716553>.
- [178] B. Andreasen, D.M. Tanenbaum, M. Hermenau, E. Voroshazi, M.T. Lloyd, Y. Galagan, B. Zimmermann, S. Kudret, W. Maes, L. Lutsen, D. Vanderzande, U. Würfel, R. Andriessen, R. Rösch, H. Hoppe, G. Teran-Escobar, M. Lira-Cantu, A. Rivaton, G.Y. Uzunoglu, D.S. Germack, M. Hösel, H.F. Dam, M. Jørgensen, S. A. Gevorgyan, M.V. Madsen, E. Bundgaard, F.C. Krebs, K. Norrman, TOF-SIMS investigation of degradation pathways occurring in a variety of organic photovoltaic devices – the ISOS-3 inter-laboratory collaboration, *Phys. Chem. Chem. Phys.* 14 (2012) 11780–11799, <https://doi.org/10.1039/C2CP41787A>.
- [179] L. Duan, Y. Zhang, M. He, R. Deng, H. Yi, Q. Wei, Y. Zou, A. Uddin, Burn-in degradation mechanism identified for small molecular acceptor-based high-efficiency nonfullerene organic solar cells, *ACS Appl. Mater. Interfaces* 12 (2020) 27433–27442, <https://doi.org/10.1021/acsami.0c05978>.
- [180] C. Wang, S. Ni, S. Braun, M. Fahrlman, X. Liu, Effects of water vapor and oxygen on non-fullerene small molecule acceptors, *J. Mater. Chem. C* 7 (2019) 879–886, <https://doi.org/10.1039/C8TC05475D>.
- [181] İ.V. Öner, E.Ç. Yilmaz, M.K. Yesilurt, G. Ömeroglu, A.N. Özakin, Operational stability and degradation of organic solar cells, *Period. Eng. Nat. Sci.* 5 (2017), <https://doi.org/10.21533/pen.v5i2.105>.
- [182] J. Adams, M. Salvador, L. Lucera, S. Langner, G.D. Spyropoulos, F.W. Fecher, M. M. Voigt, S.A. Dowland, A. Osset, H.-J. Egelhaaf, C.J. Brabec, Water ingress in encapsulated inverted organic solar cells: correlating infrared imaging and photovoltaic performance, *Adv. Energy Mater.* 5 (2015), 1501065, <https://doi.org/10.1002/aenm.201501065>.
- [183] H. Klumbies, M. Karl, M. Hermenau, R. Rösch, M. Seeland, H. Hoppe, L. Müller-Meskamp, K. Leo, Water ingress into and climate dependent lifetime of organic photovoltaic cells investigated by calcium corrosion tests, *Sol. Energy Mater. Sol. Cell.* 120 (2014) 685–690, <https://doi.org/10.1016/j.solmat.2013.10.023>.
- [184] T.S. Glen, N.W. Scarratt, H. Yi, A. Iraqi, T. Wang, J. Kingsley, A.R. Buckley, D. G. Lidzey, A.M. Donald, Grain size dependence of degradation of aluminium/calcium cathodes in organic solar cells following exposure to humid air, *Sol. Energy Mater. Sol. Cell.* 140 (2015) 25–32, <https://doi.org/10.1016/j.solmat.2015.03.015>.
- [185] K. Feron, T.J. Nagle, L.J. Rozanski, B.B. Gong, C.J. Fell, Spatially resolved photocurrent measurements of organic solar cells: tracking water ingress at edges and pinholes, *Sol. Energy Mater. Sol. Cell.* 109 (2013) 169–177, <https://doi.org/10.1016/j.solmat.2012.10.027>.
- [186] S. Zülfie, M.T. Neukom, S. Altazin, M. Zinggeler, M. Chrappa, T. Offermans, B. Ruhstaller, An effective area approach to model lateral degradation in organic solar cells, *Adv. Energy Mater.* 5 (2015), 1500835, <https://doi.org/10.1002/aenm.201500835>.
- [187] A.J. Parnell, A.J. Cadby, A.D.F. Dunbar, G.L. Roberts, A. Plumridge, R. M. Dalgleish, M.W.A. Skoda, R.A.L. Jones, Physical mechanisms responsible for the water-induced degradation of PC61BM P3HT photovoltaic thin films, *J. Polym. Sci. B Polym. Phys.* 54 (2016) 141–146, <https://doi.org/10.1002/polb.23902>.
- [188] R. Pacios, A.J. Chatten, K. Kawano, J.R. Durrant, D.D.C. Bradley, J. Nelson, Effects of photo-oxidation on the performance of poly[2-methoxy-5-(3',7'-dimethyloxy)-1,4-phenylene vinylene]:[6,6]-phenyl C61-butyric acid methyl ester solar cells, *Adv. Funct. Mater.* 16 (2006) 2117–2126, <https://doi.org/10.1002/adfm.200500714>.
- [189] E. Voroshazi, I. Cardinaletti, T. Conard, B.P. Rand, Light-induced degradation of polymer:fullerene photovoltaic devices: an intrinsic or material-dependent failure mechanism? *Adv. Energy Mater.* 4 (2014), 1400848 <https://doi.org/10.1002/aenm.201400848>.
- [190] A. Rivaton, A. Tournebize, J. Gaume, P.-O. Bussière, J.-L. Gardette, S. Therias, Photostability of organic materials used in polymer solar cells, *Polym. Int.* 63 (2014) 1335–1345, <https://doi.org/10.1002/pi.4656>.
- [191] A. Kumar, R. Devine, C. Mayberry, B. Lei, G. Li, Y. Yang, Origin of radiation-induced degradation in polymer solar cells, *Adv. Funct. Mater.* 20 (2010) 2729–2736, <https://doi.org/10.1002/adfm.201000374>.
- [192] K. Kawano, C. Adachi, Evaluating carrier accumulation in degraded bulk heterojunction organic solar cells by a thermally stimulated current technique, *Adv. Funct. Mater.* 19 (2009) 3934–3940, <https://doi.org/10.1002/adfm.200901573>.
- [193] G. Dennerl, M.C. Schärber, C.J. Brabec, Polymer-fullerene bulk-heterojunction solar cells, *Adv. Mater.* 21 (2009) 1323–1338, <https://doi.org/10.1002/adma.200801283>.
- [194] P. Cheng, Q. Shi, Y. Lin, Y. Li, X. Zhan, Evolved structure of thiazolothiazole based small molecules towards enhanced efficiency in organic solar cells, *Org. Electron.* 14 (2013) 599–606, <https://doi.org/10.1016/j.orgel.2012.11.026>.
- [195] L. Dou, C.-C. Chen, K. Yoshimura, K. Ohya, W.-H. Chang, J. Gao, Y. Liu, E. Richard, Y. Yang, Synthesis of 5H-Dithieno[3,2-b;3',2'-d]pyran as an electron-rich building block for donor–acceptor type low-bandgap polymers, *Macromolecules* 46 (2013) 3384–3390, <https://doi.org/10.1021/ma400452j>.
- [196] X. Zhan, Z. Tan, B. Domercq, Z. An, X. Zhang, S. Barlow, Y. Li, D. Zhu, B. Kippelen, S.R. Marder, A high-mobility electron-transport polymer with broad absorption and its use in field-effect transistors and all-polymer solar cells, *J. Am. Chem. Soc.* 129 (2007) 7246–7247, <https://doi.org/10.1021/ja071760d>.
- [197] N. Chander, S. Singh, S.S.K. Iyer, Stability and reliability of P3HT:PC61BM inverted organic solar cells, *Sol. Energy Mater. Sol. Cell.* 161 (2017) 407–415, <https://doi.org/10.1016/j.solmat.2016.12.020>.
- [198] B.C. Thompson, J.M.J. Fréchet, Polymer–fullerene composite solar cells, *Angew. Chem. Int. Ed.* 47 (2008) 58–77, <https://doi.org/10.1002/anie.200702506>.
- [199] I. Fraga Dominguez, A. Distler, L. Lüer, Stability of organic solar cells: the influence of nanostructured carbon materials, *Adv. Energy Mater.* 7 (2017), 1601320, <https://doi.org/10.1002/aenm.201601320>.
- [200] T.L. Nguyen, T.H. Lee, B. Gautam, S.Y. Park, K. Gundogdu, J.Y. Kim, H.Y. Woo, Single component organic solar cells based on oligothiophene–fullerene conjugate, *Adv. Funct. Mater.* 27 (2017), 1702474, <https://doi.org/10.1002/adfm.201702474>.
- [201] M. Nam, J. Yoo, Y. Park, H.Y. Noh, Y. Park, J. Cho, J.-A. Kim, J. Kim, H.H. Lee, R. Chang, D.-H. Ko, Ternary blend organic solar cells with improved morphological stability, *J. Mater. Chem. A* 7 (2019) 9698–9707, <https://doi.org/10.1039/C9TA00382G>.
- [202] W. Greenbank, L. Hirsch, G. Wantz, S. Chambon, Interfacial thermal degradation in inverted organic solar cells, *Appl. Phys. Lett.* 107 (2015), 263301, <https://doi.org/10.1063/1.4938554>.
- [203] T. Wang, A.J. Pearson, A.D.F. Dunbar, P.A. Stanić, D.C. Watters, H. Yi, A.J. Ryan, R.A.L. Jones, A. Iraqi, D.G. Lidzey, Correlating structure with function in thermally annealed PCDTBT:PC70BM photovoltaic blends, *Adv. Funct. Mater.* 22 (2012) 1399–1408, <https://doi.org/10.1002/adfm.201102510>.
- [204] J. Jo, S.-S. Kim, S.-I. Na, B.-K. Yu, D.-Y. Kim, Time-dependent morphology evolution by annealing processes on polymer:fullerene blend solar cells, *Adv. Funct. Mater.* 19 (2009) 866–874, <https://doi.org/10.1002/adfm.200800968>.
- [205] W. Farooq, M.A. Musarat, J. Iqbal, S.A.A. Kazmi, A.D. Khan, W.S. Alaloul, A. O. Baarimah, A.Y. Elnaggag, S.S.M. Ghoneim, R.N.R. Ghaly, Optimized thin-film organic solar cells with enhanced efficiency, *Sustainability* 13 (2021), 13087, <https://doi.org/10.3390/su132313087>.

- [206] W. Yang, Z. Luo, R. Sun, J. Guo, T. Wang, Y. Wu, W. Wang, J. Guo, Q. Wu, M. Shi, H. Li, C. Yang, J. Min, Simultaneous enhanced efficiency and thermal stability in organic solar cells from a polymer acceptor additive, *Nat. Commun.* 11 (2020) 1218, <https://doi.org/10.1038/s41467-020-14926-5>.
- [207] S. Bertho, I. Haeldermans, A. Swinnen, W. Moens, T. Martens, L. Lutsen, D. Vanderzande, J. Manca, A. Senes, A. Bonfiglio, Influence of thermal ageing on the stability of polymer bulk heterojunction solar cells, *Sol. Energy Mater. Sol. Cell.* 91 (2007) 385–389, <https://doi.org/10.1016/j.solmat.2006.10.008>.
- [208] S. Savagatrup, A.D. Printz, T.F. O'Connor, A.V. Zaretski, D. Rodriguez, E. J. Sawyer, K.M. Rajan, R.I. Acosta, S.E. Root, D.J. Lipomi, Mechanical degradation and stability of organic solar cells: molecular and microstructural determinants, *Energy Environ. Sci.* 8 (2014) 55–80, <https://doi.org/10.1039/C4EE02657H>.
- [209] S.R. Dupont, M. Oliver, F.C. Krebs, R.H. Dauskardt, Interlayer adhesion in roll-to-roll processed flexible inverted polymer solar cells, *Sol. Energy Mater. Sol. Cell.* 97 (2012) 171–175, <https://doi.org/10.1016/j.solmat.2011.10.012>.
- [210] P. Cheng, X. Zhan, Stability of organic solar cells: challenges and strategies, *Chem. Soc. Rev.* 45 (2016) 2544–2582, <https://doi.org/10.1039/C5CS00593K>.
- [211] C. Bruner, F. Novoa, S. Dupont, R. Dauskardt, Decohesion kinetics in polymer organic solar cells, *ACS Appl. Mater. Interfaces* 6 (2014) 21474–21483, <https://doi.org/10.1021/am506482q>.
- [212] F. Nickel, T. Haas, E. Wegner, D. Bahro, S. Salehin, O. Kraft, P.A. Gruber, A. Colsmann, Mechanically robust, ITO-free, 4.8% efficient, all-solution processed organic solar cells on flexible PET foil, *Sol. Energy Mater. Sol. Cell.* 130 (2014) 317–321, <https://doi.org/10.1016/j.solmat.2014.07.005>.
- [213] M. Hösel, R.R. Søndergaard, M. Jørgensen, F.C. Krebs, Failure modes and fast repair procedures in high voltage organic solar cell installations, *Adv. Energy Mater.* 4 (2014) 1301625, <https://doi.org/10.1002/aenm.201301625>.
- [214] O. Awartani, B.I. Lemanski, H.W. Ro, L.J. Richter, D.M. DeLongchamp, B. T. O'Connor, Correlating stiffness, ductility, and morphology of polymer:fullerene films for solar cell applications, *Adv. Energy Mater.* 3 (2013) 399–406, <https://doi.org/10.1002/aenm.201200595>.
- [215] L. Duan, A. Uddin, Progress in stability of organic solar cells, *Adv. Sci.* 7 (2020), 1903259, <https://doi.org/10.1002/adv.201903259>.
- [216] S. Dey, P. Vivo, A. Efimov, H. Lemmetyinen, Enhanced performance and stability of inverted organic solar cells by using novel zinc-benzothiazole complexes as anode buffer layers, *J. Mater. Chem. A* 21 (2011) 15587–15592, <https://doi.org/10.1039/C1JM13256C>.
- [217] R. Peng, T. Yan, J. Chen, S. Yang, Z. Ge, M. Wang, Passivating surface defects of n-SnO₂ electron transporting layer by InP/ZnS quantum dots: toward efficient and stable organic solar cells, *Advanced Electronic Materials* 6 (2020), 1901245, <https://doi.org/10.1002/aelm.201901245>.
- [218] S. Rafique, N.A. Roslan, S.M. Abdullah, L. Li, A. Supangat, A. Jilani, M. Iwamoto, UV-ozone treated graphene oxide/PEDOT:PSS bilayer as a novel hole transport layer in highly efficient and stable organic solar cells, *Org. Electron.* 66 (2019) 32–42, <https://doi.org/10.1016/j.orgel.2018.12.005>.
- [219] R. Yu, H. Yao, L. Hong, Y. Qin, J. Zhu, Y. Cui, S. Li, J. Hou, Design and application of volatilizable solid additives in non-fullerene organic solar cells, *Nat. Commun.* 9 (2018) 4645, <https://doi.org/10.1038/s41467-018-07017-z>.
- [220] I.A. Channa, A. Distler, M. Zaiser, C.J. Brabec, H.-J. Egelhaaf, Thin film encapsulation of organic solar cells by direct deposition of polysilazanes from solution, *Adv. Energy Mater.* 9 (2019), 1900598, <https://doi.org/10.1002/aenm.201900598>.
- [221] S.-H. Lee, J.-W. Seo, J.-Y. Lee, Stable inverted small molecular organic solar cells using a p-doped optical spacer, *Nanoscale* 7 (2014) 157–165, <https://doi.org/10.1039/C4NR05425C>.
- [222] J.-L. Lan, S.-J. Cherng, Y.-H. Yang, Q. Zhang, S. Subramaniyan, F.S. Ohuchi, S. A. Jenekhe, G. Cao, The effects of Ta₂O₅–ZnO films as cathodic buffer layers in inverted polymer solar cells, *J. Mater. Chem. A* 2 (2014) 9361–9370, <https://doi.org/10.1039/C4TA01350F>.
- [223] S. Lattante, Electron and hole transport layers: their use in inverted bulk heterojunction polymer solar cells, *Electronics* 3 (2014) 132–164, <https://doi.org/10.3390/electronics3010132>.
- [224] Y. Wang, W. Lan, N. Li, Z. Lan, Z. Li, J. Jia, F. Zhu, Stability of nonfullerene organic solar cells: from built-in potential and interfacial passivation perspectives, *Adv. Energy Mater.* 9 (2019), 1900157, <https://doi.org/10.1002/aenm.201900157>.
- [225] S. Wu, S. Han, Y. Zheng, H. Zheng, N. Liu, L. Wang, Y. Cao, J. Wang, pH-neutral PEDOT:PSS as hole injection layer in polymer light emitting diodes, *Org. Electron.* 12 (2011) 504–508, <https://doi.org/10.1016/j.orgel.2010.12.015>.
- [226] S. Jung, J. Lee, U. Kim, H. Park, Solution-processed molybdenum oxide with hydroxyl radical-induced oxygen vacancy as an efficient and stable interfacial layer for organic solar cells, *Solar RRL* 4 (2020), 1900420, <https://doi.org/10.1002/solr.201900420>.
- [227] H. Cao, W. He, Y. Mao, X. Lin, K. Ishikawa, J.H. Dickerson, W.P. Hess, Recent progress in degradation and stabilization of organic solar cells, *J. Power Sources* 264 (2014) 168–183, <https://doi.org/10.1016/j.jpowsour.2014.04.080>.
- [228] Z. Zheng, S. Zhang, J. Wang, J. Zhang, D. Zhang, Y. Zhang, Z. Wei, Z. Tang, J. Hou, H. Zhou, Exquisite modulation of ZnO nanoparticle electron transporting layer for high-performance fullerene-free organic solar cell with inverted structure, *J. Mater. Chem. A* 7 (2019) 3570–3576, <https://doi.org/10.1039/C8TA11624E>.
- [229] Y. Sun, J.H. Seo, C.J. Takacs, J. Seifter, A.J. Heeger, Inverted polymer solar cells integrated with a low-temperature-annealed sol-gel-derived ZnO film as an electron transport layer, *Adv. Mater.* 23 (2011) 1679–1683, <https://doi.org/10.1002/adma.201004301>.
- [230] S. Park, H. Ahn, J. Kim, J.B. Park, J. Kim, S.H. Im, H.J. Son, High-performance and stable nonfullerene acceptor-based organic solar cells for indoor to outdoor light, *ACS Energy Lett.* 5 (2020) 170–179, <https://doi.org/10.1021/acsenergylett.9b01819>.
- [231] N. Gasparini, S.H.K. Paletti, J. Bertrandie, G. Cai, G. Zhang, A. Wadsworth, X. Lu, H.-L. Yip, I. McCulloch, D. Baran, Exploiting ternary blends for improved photostability in high-efficiency organic solar cells, *ACS Energy Lett.* 5 (2020) 1371–1379, <https://doi.org/10.1021/acsenergylett.0c00604>.
- [232] A. Wadsworth, R.S. Ashraf, M. Abdelsamie, S. Pont, M. Little, M. Moser, Z. Hamid, M. Neophytou, W. Zhang, A. Amassian, J.R. Durrant, D. Baran, I. McCulloch, Highly efficient and reproducible nonfullerene solar cells from hydrocarbon solvents, *ACS Energy Lett.* 2 (2017) 1494–1500, <https://doi.org/10.1021/acsenergylett.7b00390>.
- [233] H. Lin, L. Yang, Q. Chen, X. Kong, X. Du, W. Zhao, Z. Wang, C. Zheng, S. Tao, Q. Tong, An universal morphology regulator for efficient and stable nonfullerene organic solar cells by π–π interaction, *Org. Electron.* 86 (2020), 105827, <https://doi.org/10.1016/j.orgel.2020.105827>.
- [234] D. Elkington, N. Cooling, X.J. Zhou, W.J. Belcher, P.C. Dastoor, Single-step annealing and encapsulation for organic photovoltaics using an exothermically-setting encapsulant material, *Sol. Energy Mater. Sol. Cell.* 124 (2014) 75–78, <https://doi.org/10.1016/j.solmat.2014.01.039>.